

THESIS

USING TOTAL PRECIPITABLE WATER ANOMALY AS A FORECAST AID FOR HEAVY
PRECIPITATION EVENTS

Submitted by

Lance M. VandenBoogart

Department of Atmospheric Science

In partial fulfillment of the requirements

For the Degree of Master of Science

Colorado State University

Fort Collins, Colorado

Spring 2013

Master's Committee:

Advisor: Thomas H. Vonder Haar

Russ S. Schumacher
Jorge A. Ramírez
Stanley Q. Kidder

Copyright by Lance M. VandenBoogart 2013

All Rights Reserved

ABSTRACT

USING TOTAL PRECIPITABLE WATER ANOMALY AS A FORECAST AID FOR HEAVY PRECIPITATION EVENTS

Heavy precipitation events are of interest to weather forecasters, local government officials, and the Department of Defense. These events can cause flooding which endangers lives and property. Military concerns include decreased trafficability for military vehicles, which hinders both war- and peace-time missions. Even in data-rich areas such as the United States, it is difficult to determine when and where a heavy precipitation event will occur. The challenges are compounded in data-denied regions. The hypothesis that total precipitable water anomaly (TPWA) will be positive and increasing preceding heavy precipitation events is tested in order to establish an understanding of TPWA evolution. Results are then used to create a precipitation forecast aid.

The operational, 16 km-gridded, 6-hourly TPWA product developed at the Cooperative Institute for Research in the Atmosphere (CIRA) compares a blended TPW product with a TPW climatology to give a percent of normal TPWA value. TPWA evolution is examined for 84 heavy precipitation events which occurred between August 2010 and November 2011. An algorithm which uses various TPWA thresholds derived from the 84 events is then developed and tested using dichotomous contingency table verification statistics to determine the extent to which satellite-based TPWA might be used to aid in forecasting precipitation over mesoscale domains.

The hypothesis of positive and increasing TPWA preceding heavy precipitation events is supported by the analysis. Event-average TPWA rises for 36 hours and peaks at 154% of normal at the event time. The average precipitation event detected by the forecast algorithm is not of sufficient magnitude to be termed a “heavy” precipitation event; however, the algorithm adds skill to a climatological precipitation forecast. Probability of detection is low and false alarm ratios are large, thus qualifying the algorithm’s current use as an aid rather than a deterministic forecast tool. The algorithm’s ability to be easily modified and quickly run gives it potential for future use in precipitation forecasting.

ACKNOWLEDGEMENTS

This research would not have been possible without the generous support of several individuals. I would like to thank my advisor, Tom Vonder Haar, for inviting me to be a part of his research group at Colorado State University, and for his help in developing a thesis topic that aligns well with my career goals. I thank John Forsythe for spending many hours introducing me to the world of coding and for supporting me through CIRA by providing much of the data used in this work. Thanks to committee member Russ Schumacher for helping me with precipitation analysis, both directly through meetings and indirectly through his archive of heavy precipitation events. Thanks to committee members Stan Kidder and Jorge Ramírez for their insight and time spent reviewing this thesis.

Many others also contributed to this work from behind the scenes. First, I thank the Lord God for providing me with a sharp mind and the grace to use it for this research. I thank my parents and siblings for their love and support throughout my time in graduate school. Thanks to my girlfriend, Shaina Lex, for her patience, willingness to listen, and desire to help in any way possible. Finally, thanks to my peers at the Atmospheric Science department of Colorado State University, especially my officemates, Eric Guillot, Gavin Roy, and Kim Erickson, for making my time here an enjoyable one.

This research was supported by the Department of Defense Center for Geosciences/Atmospheric Research at Colorado State University under Cooperative Agreement W911NF-06-2-0015 with the Army Research Laboratory.

TABLE OF CONTENTS

Abstract.....	ii
Acknowledgements.....	iv
Table of Contents.....	v
1. Introduction.....	1
2. Literature Review.....	6
2.1 Overview of Passive Microwave Remote Sensing of Water Vapor.....	6
2.2 Total Precipitable Water.....	7
2.3 Heavy Precipitation Events.....	11
2.4 Using Anomalies as a Forecast Aid.....	15
3. Instrumentation and Data Products.....	22
3.1 Blended TPW.....	22
3.2 NVAP Climatology.....	25
3.3 Total Precipitable Water Anomaly.....	26
3.4 Stage IV Precipitation.....	28
4. Methodology.....	34
4.1 Heavy Precipitation Event Analysis.....	34
4.2 Domain Considerations.....	36
4.3 Temporal Considerations.....	38
4.4 Data Quality Assurance.....	39
4.5 Forecasting with TPWA.....	40

5. Results.....	51
5.1 Composite Heavy Precipitation Events	51
5.2 Forecast Tool Verification	54
6. Summary and Conclusions	64
6.1 Research Conclusions	64
6.2 Research Limitations	65
6.3 Future Work	67
References.....	73
Appendix I	78
List of Abbreviations	83

1. INTRODUCTION

Heavy precipitation events have wide-ranging societal and economic ramifications; yet forecasting these events more than a few hours beforehand remains a challenge. Civilian weather forecasters are interested in any heavy precipitation event which may lead to flooding in the communities they serve. The military's concern with heavy rainfall revolves around their requirement to assess the battlespace and all variables affecting the mission at hand. Situational awareness is essential for these groups who have the responsibility to protect lives and provide forecast information to customers.

Flooding is a major concern related to heavy precipitation. Flood damage has averaged \$7.82 billion annually in the United States of America (U.S.) over the past 30 years according to the National Weather Service (NWS) (NWS 2012). On average, a sobering 81 fatalities occur per year directly due to freshwater flooding (Ashley and Ashley 2008; Fig. 1.1). Forecasters cannot prevent all losses from occurring; the circumstances leading to these losses are complex and largely out of the forecaster's control. Yet studies have shown that advance warning can help those in the path of extreme weather prepare for the imminent danger, thus reducing negative consequences (Simmons and Sutter 2008). Although great advances in warning systems have been made in recent decades, there is still room for improvement. Collaborative research projects are one proven source of such improvement, increasing the probability of detection and lead times for both severe thunderstorm and flash flood warnings issued by the NWS (Waldstreicher 2005).

The best precipitation forecast utilizes all available data due to the complexity of the atmospheric processes involved. The U.S. has a relatively dense array of meteorological data available operationally with which to make forecasts. Doppler radars, satellites, radiosondes,

ground observing stations, and numerical weather prediction models all assist in ascertaining the current state of the atmosphere. But not all these tools are available to every forecaster (Fig. 1.2); especially lacking are those forecasting for ocean regions or countries without a coordinated meteorological service. Heavy rain events still occur in these so-called “data-denied” regions, but the tools available to assess the potential danger are limited.

Data-denied regions are of particular interest to the military, since they often operate in the global theatre. Precipitation forecasts still must be made in order to ensure the safety and success of both wartime and humanitarian missions, even where dense data coverage is not available. The U.S. Department of Defense views heavy precipitation as a potential threat to the success of these missions. Trafficability becomes a concern when heavy precipitation occurs, as tanks and other military vehicles are hindered by wet soil and standing water. Dam failure is another hazard. The U.S. Army Corps of Engineers (USACE) is continually working to ensure the safety of aging dams and other water retaining structures around the world for the protection of populations downstream (USACE 2011). The military uses the Tri-Service Integrated Weather Effects Decision Aid (T-IWEDA) software package to assess the level of risk that weather presents. T-IWEDA ingests many atmospheric variables, including atmospheric moisture, to give an overall impact output. Additional data regarding rainfall potential could improve this mission-based risk assessment (Shirkey 2010).

Understanding the variables and interactions which dictate heavy precipitation events help decision makers in the public, private, and military sectors make informed decisions and accurate forecasts, helping to protect lives and property. Total precipitable water (TPW) is one variable which modulates the likelihood of occurrence and the intensity of precipitation. TPW is a useful quantity to consider when analyzing precipitation systems because it is a measure of the

cumulative water vapor content of the atmosphere. Large amounts of water vapor are needed to produce heavy precipitation, whereas an atmosphere with sparse water vapor limits extreme rainfall accumulations. TPW anomaly (TPWA) is an extension of TPW which relates the current value to a quantitative measure of the average for a given location and time of year. One might expect increasing TPW/TPWA to be indicative of an increasing chance of heavy rainfall. This conventional wisdom is closely related to the hypothesis of this research: Total precipitable water anomaly will be positive and increasing preceding a heavy precipitation event.

Water vapor must be present in rising air parcels for condensation to occur. Furthermore, parcels of air containing water vapor are more buoyant than equivalent dry parcels (Petty 2007). Yet it is well-understood that it takes more than water vapor to cause precipitation; moisture is a necessary, but insufficient, atmospheric component in the creation of precipitation. Other atmospheric ingredients must often assist in the process; convection, horizontal flow over orography, and other dynamic sources of lift play a major role in precipitating systems (Doswell et al. 1996; Martin 2006). Cloud microphysical properties, such as the presence or lack of abundant cloud condensation nuclei, can also affect the nature of precipitation (Orville 2003). These additional variables are not examined in this work since the objective is to better understand what can be gleaned from water vapor distribution alone. The hypothesis tests the strength of the connection between TPWA and heavy precipitation as it pertains to forecasting.

The TPWA dataset analyzed is ideally suited to test the hypothesis while keeping the aforementioned forecaster priorities in mind. The National Oceanic and Atmospheric Administration (NOAA) operational TPWA product is based solely on satellite inputs connected to a TPW climatology. This makes it ideal for data-denied regions where more conventional observing systems are not in place. The product is quasi-global, allowing it to be used in nearly

any area of interest, with the exception being latitudes poleward of 71°N or 71°S . The TPWA product also has the potential to add additional insight for forecasters in the U.S. and other data-rich areas. A strong connection between TPWA and precipitation in the day preceding an event could potentially be exploited to provide the forecaster with additional information in the time period between radar-based nowcasts (0-6 hour forecasts) and longer-term model forecasts. TPWA values are given as a “percentage of normal”, thus making interpretation simple for users.

This research investigates the extent to which TPWA can be used as a regional forecast aid in the time period leading up to a heavy precipitation event. This is accomplished by analyzing a state-of-the-art TPWA dataset in domains surrounding 84 heavy precipitation events that occurred throughout 2010 and 2011. Events which cross an intensity threshold are compiled and summarized statistically. A signal of positive, increasing TPWA leading up to the heavy precipitation events supports the hypothesis, suggesting a TPWA-based forecast tool may be useful. Little to no signal in TPWA would suggest there are too many complicating factors for TPWA to be used alone as a forecasting aid. A forecasting tool/algorithm with many tunable parameters is then developed and tested in an attempt to predict precipitation events across the central to eastern United States.

Literature which establishes the basis for this research is reviewed in chapter 2. Chapter 3 details the satellite-based data products which have been used to create TPWA, the TPWA dataset itself, and the verification precipitation dataset. Chapter 4 covers the methodology used to test the hypothesis via heavy precipitation event analysis. Subsequently it describes the methodology used in developing the forecasting algorithm. Chapter 5 highlights the results of the heavy precipitation event analysis and the forecasting tool verification. A summary with conclusions, limitations, and ideas for expanding this work are discussed in chapter 6.

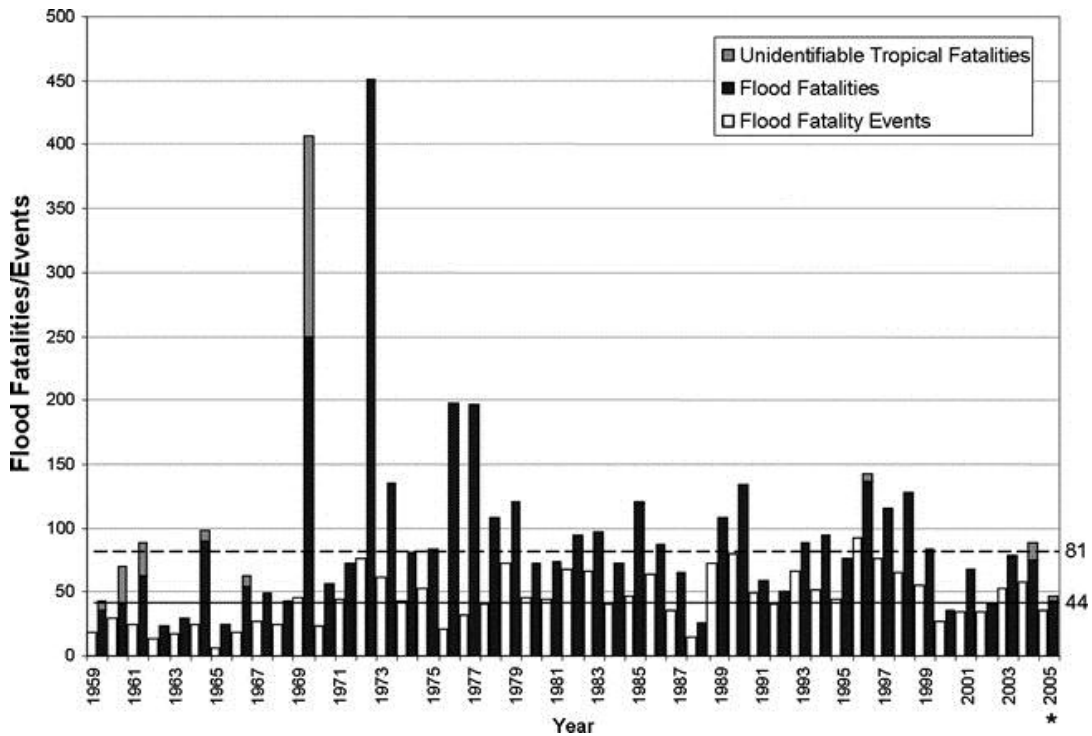


Figure 1.1: Flood fatalities (black bars) and number of fatal flood events (white bars) from 1959 to 2005. (reproduced from Ashley and Ashley 2008)

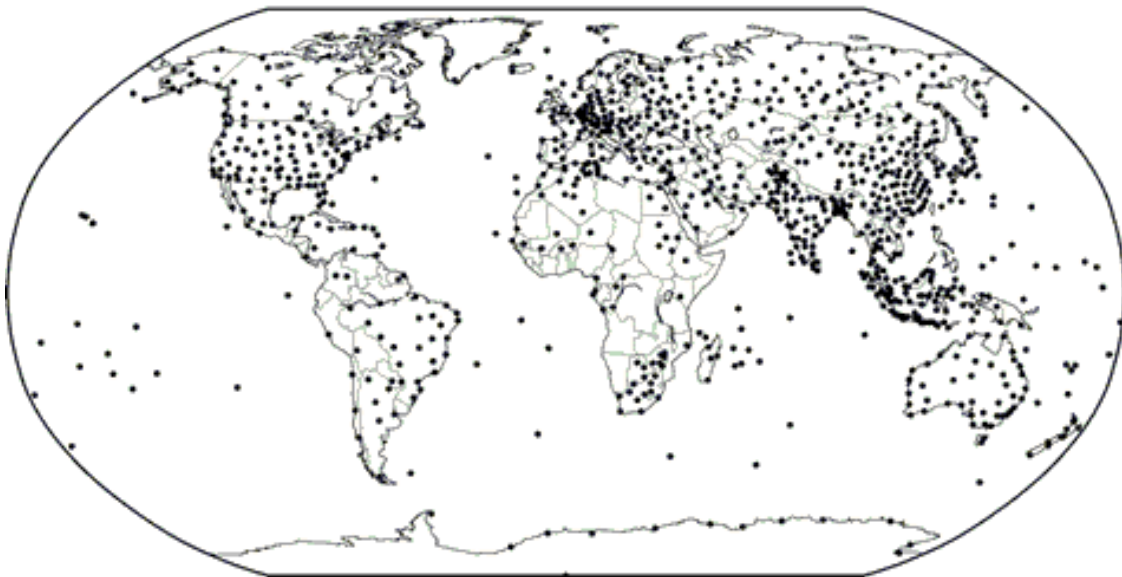


Figure 1.2: Global atmospheric sounding locations that were active as of 2003, used as a proxy for global data coverage. Note the large gaps over the oceans, Africa, and parts of the Middle East. (reproduced from Durre et al. 2006)

2. LITERATURE REVIEW

2.1 Overview of Passive Microwave Remote Sensing of Water Vapor

Water vapor has a complex electromagnetic radiation absorption spectrum due to its non-linear molecular structure and electric dipole moment. Atmospheric remote sensing techniques utilize these complexities to determine atmospheric variables, such water vapor content, via satellite. The Soviet Kosmos 243 satellite, launched in 1968, carried the first satellite-based microwave radiometer capable of making quantitative water vapor measurements. Early U.S. satellites which could make this measurement included Nimbus 5, 6, and 7, Seasat, and Defense Metrological Satellite Program (DMSP) satellites (Kidder and Vonder Haar 1995). Currently the NOAA-, DMSP-, and MetOp-series of polar-orbiting satellites make operational water vapor measurements.

Water vapor weakly absorbs microwave radiation, and the scattering of microwave radiation by non-precipitating drops is negligible. There is a weak water vapor rotational absorption line in the electromagnetic spectrum at 22.235 GHz (Fig. 2.1). Relatively clean atmospheric windows, i.e. regions of the spectrum with little absorption, border this absorption line. Exploiting the difference in retrieved brightness temperature between the peak channel (a small portion of the spectrum sampled near 22.235 GHz) and a window channel (often near 31 GHz) allows water vapor content to be retrieved. More precisely, the Rayleigh-Jeans law is applied to the integrated form of Schwarzschild's equation, as detailed by Grody et al. (1980) and Kidder and Vonder Haar (1995). Using the fact that both cloud liquid water and TPW absorb microwave radiation differently at 22 and 31 GHz, one can back out the values for each of these variable using a simultaneous retrieval method with a few assumptions. A sea surface temperature (SST), surface emittance, and atmospheric transmittance must be known or

assumed. Surface temperature and transmittance are approximated without issue, and more recent retrievals even specify SSTs. However, surface emittance is a strong function of surface type, and this method cannot be used if surface emittance is strongly fluctuating or close to one over a scene: TPW retrievals by this method must be done over a uniform surface with low emittance. The ocean provides an ideal backdrop with uniform, cold brightness temperatures due to the low emittance of water. Adding water vapor to a scene increases the brightness temperature measured by satellite radiometers. Measuring this brightening quantitatively allows for a TPW amount to be determined.

After a few assumptions described by Kidder and Vonder Haar (1995), cloud liquid water (U_L) and TPW (U_V) can be retrieved since they are linear combinations of the $\mu \ln[T_s - T_B(22)]$ term in the following system of equations:

$$U_L = a_{22}\mu \ln[T_s - T_B(22)] + a_{31}\mu \ln[T_s - T_B(31)] + a_0$$

$$U_V = b_{22}\mu \ln[T_s - T_B(22)] + b_{31}\mu \ln[T_s - T_B(31)] + b_0 ,$$

where T_s is the background surface temperature, T_B is the measure brightness temperature measured by a satellite radiometer, μ is the cosine of the viewing zenith angle, and a and b are coefficients which can be determined using a radiative model, or by comparing with observations of TPW taken by independent instruments.

2.2 Total Precipitable Water

Precipitable water (PW) is defined by the American Meteorological Society (AMS) as “The total atmospheric water vapor contained in a vertical column of unit cross-sectional area extending between any two specified levels” (AMS Glossary 2012). It has units of kg m^{-2} , but is

more often expressed in length units, with values expressing the equivalent depth of water that would result over the unit cross-sectional area if the water vapor were condensed. The term “total” is often added to “precipitable water” to specify that the quantity is taken over the entire depth of the atmosphere, from the earth’s surface to the top of the atmosphere.

It is worthwhile to investigate the climatology of TPW to get a sense of average global distribution. An early climatology by Tuller (1968) notes some key features of global TPW using data from 182 ground stations. His results are informative, despite the lack of observations compared to today’s datasets. A general latitudinal gradient is discovered, with the highest values over the equator, and lowest values over the poles (Fig. 2.2). This is as expected since the saturation vapor pressure of liquid water is a function of temperature by thermodynamic principles (Petty 2007). Continents are drier than oceans, as they lack the proximate water surface source provided by the ocean. The winter is drier than summer, as increased temperature provides more ambient moisture via evaporation. The largest annual variability occurs in the Bay of Bengal, and the lowest variability is over the tropical Pacific. The Bay of Bengal is affected by the Indian monsoon, so despite being a warm ocean region, advection of relatively dry air masses during winter leads to high variability. The tropical Pacific, on the other hand, has consistently high values resulting from bountiful solar radiation, warm surface temperatures, and ocean sources in all directions, which in tandem lead to small variability.

The added frequency and spatial coverage afforded by satellite-based instruments make finer-scale phenomena more evident. Ferraro et al. (1996) generate plots of global monthly-mean TPW values using the satellite-based Special Sensor Microwave/Imager (SSM/I) (Fig. 2.3). The measurements reveal a number of features not observable in Tuller’s earlier research. Among these are dry regions off the western coasts of continents, which are present due to both oceanic

upwelling of cool water and dry atmospheric subsidence. These oceanic subtropical zones are often called “oceanic deserts” due to their relatively low TPW values and rainfall frequencies. A seasonal latitudinal shift toward the summer hemisphere in the equatorial band of high TPW values is noted, as is evidence of a monsoonal circulation near India.

Presently there are many TPW climatologies available. Amenu and Kumar (2005) compared two recent TPW climatologies: the National Aeronautics and Space Administration (NASA) Water Vapor Project (NVAP) (Randel et al. 1996) and the National Centers for Environmental Prediction (NCEP) – National Center for Atmospheric Research (NCAR) Reanalysis-2 project (Kanamitsu et al. 2002). The two datasets overlap for a 12-year period between 1988 and 1999. Discrepancies include Reanalysis-2’s depiction of a wetter atmosphere than NVAP, more notably in winter, and NVAP’s higher spatial and temporal variability. Besides these notable differences, the datasets exhibit a high correlation and have a qualitatively similar pattern. Interseasonal variability is found to be more pronounced than interannual variability in both. Furthermore, much of the interannual variability is attributable to ENSO, while the interseasonal variability is heavily influenced by monsoonal circulations. The overall agreement between NVAP (Randel et al. 1996) and Reanalysis-2 (Kanamitsu et al. 2002) is encouraging for this present study, since two independent methodologies producing similar results increases one’s confidence that the first-order physics of atmospheric water vapor are being represented well in the NVAP dataset.

There are interesting and well-studied features of TPW that go beyond general climatology. Atmospheric rivers are bands of high TPW which are typically a few hundred kilometers wide and can stretch over thousands of kilometers (Bao et al. 2006; Fig. 2.4). They commonly occur along mid-latitude cyclone cold fronts in the pre-frontal “warm conveyor belt”,

otherwise known as the low-level jet (LLJ), which is described in detail by Browning and Pardoe (1973). Typical water vapor fluxes in an atmospheric river are approximately $150 \times 10^6 \text{ kg s}^{-1}$, which is comparable to flow rates in major terrestrial rivers, such as the Amazon (Newell and Zhu 1992).

Atmospheric rivers bridge the weather-climate interface. While important for tropical oceanic water vapor export on climatological time scales, they are also of interest to the forecaster over synoptic time scales. Atmospheric rivers supply moisture for orographically-forced heavy precipitation events. White et al. (2003) used an upward-pointing Doppler radar to examine precipitation characteristics of land-falling atmospheric rivers in California. The moist, LLJs which orthogonally intersected terrain lead to quasi-steady, shallow rain processes in 28% of the cases observed. The mean rain rate for the LLJ cases was 3.95 mm h^{-1} , but values as high as 20 mm h^{-1} were observed. Knowing where these rivers are is invaluable for forecasters in locations upstream of mountain ranges, such as the western California coast. In the case of California, the beam-blocking by local topography makes traditional NWS radar precipitation surveillance difficult, increasing the usefulness of a satellite-based TPW product for anticipating and even “nowcasting” (0-6 hr forecasting) precipitation events.

Additionally, atmospheric rivers can provide fuel for rapid intensification in extratropical cyclones. Zhu and Newell (1994) studied this phenomenon, and found an association between cyclone movement/intensification and the position of the leading edge of atmospheric rivers. Moisture provided by the rivers tends to deepen cyclones if the cyclone centers remain collocated with an atmospheric river’s leading edge. Latent heat release during condensation causes atmospheric heating thus intensifying local upward vertical motion. Another effect of such a rich source of water vapor is additional precipitation amounts. Rivers supply much of the

moisture for precipitation in such systems. Newell and Zhu (1994) further apply knowledge of atmospheric rivers to ice core formation by speculating on a connection between global temperature changes in the past and the frequency of atmospheric river occurrence, thus demonstrating novel atmospheric river applications.

Although atmospheric rivers are not explicitly examined in this current research, they are important because they are often a source of large TPWA values. Understanding where atmospheric rivers are located and which atmospheric systems produce them is key to physically understanding the mechanisms which often cause anomalously high TPW.

TPW climatologies and average distributions are useful for understanding climate, yet the spatial variability and local microclimates of a given region complicate the work of forecasters who need to predict heavy precipitation, especially for those without extensive experience. If a plume of 40 mm TPW values is moving northward during March for the forecaster in Afghanistan, should the meteorologist tasked to forecast for this region expect any significant weather? It may be difficult to know, but having an operational product that incorporates local and seasonal climatology helps remove uncertainty. The TPWA product used in this research includes such a climatology.

2.3 Heavy Precipitation Events

Heavy precipitation events are often studied in the context of flash flood events since loss of life and property are more directly connected with the latter. Hydrological conditions at a given location modulate the amount of rain which will cause a flash flood, yet heavy precipitation is often intimately related to flash flooding. A given rainfall event's chance to produce a flash flood is affected by factors such as antecedent precipitation, size of the drainage basin, topography, amount of urban use, and many other factors (Doswell et al. 1996). Although

these considerations are very important for flash flood forecasting, the following studies focus on the meteorological aspects of flash floods (i.e. heavy precipitation), thus providing a context for understanding what causes heavy precipitation events.

There are many ingredients which must come together for heavy precipitation events to occur. Maddox et al. (1979) identify a number of features common in many of 151 non-tropical flash flood events. Storms are convective in nature with cells repeatedly forming and moving over the same area. They occur in regions with a high surface dew point, and have relatively high moisture contents through a deep tropospheric layer. Weak to moderate vertical shear of the horizontal wind is present while weak mid-tropospheric meso- α troughs often help trigger storms under presiding large-scale mid-tropospheric ridges. The studied flash flood events were more common in the overnight hours, making them particularly dangerous. The authors also note the benign surface patterns and large variability of winds aloft which make the forecasting of heavy precipitation difficult.

Doswell et al. (1996) focus on the meteorological processes involved in heavy precipitation to determine the necessary ingredients. A simple summary statement by the authors brings the important issues to light: “The heaviest precipitation occurs where the rainfall rate is the highest for the longest time.”. High precipitation rates occur where moist air is lifted to condensation. Faster ascent rates or larger amounts of water vapor in rising air parcels lead to greater precipitation rates, with precipitation efficiency scaling the overall effect. Duration is the other key issue, with storm structure and system motion vectors both playing major roles. Long durations are associated with systems which have either slow movement or a large area of high rainfall rates along their motion vectors, or a combination of both. Figure 2.5 demonstrates

possible combinations of these effects at a point location. Systems with high rainfall rates in linear bands with cell motions nearly parallel to the mean wind cause the highest accumulations.

Mesoscale Convective Systems (MCSs) are one category of weather systems which often cause heavy precipitation in mid-latitudes. When dividing extreme rainfall events into three categories (synoptic, tropical, or MCS), Schumacher and Johnson (2006) quantitatively find that 66% of 184 heavy rain events in the central and eastern U.S. during 1999-2003 occur due to MCSs. This percentage increases to 74% when examining only the warm season.

MCSs have a variety of structures, but two commonly observed in heavy precipitation cases are the Training Line/Adjoining Stratiform (TL/AS) and the Backbuilding/Quasi-stationary (BB) structures (Fig. 2.6), as defined by Schumacher and Johnson (2005) in their study of 116 heavy rain events. TL/AS MCSs are linear in nature with cell motion approximately parallel to the convective line. Most form on the cool side of a synoptic-scale warm or stationary front, with southerly surface winds south of the extreme rainfall center and weak easterly winds north of the center. BB MCSs are characterized by convective cells repeatedly forming upstream of their predecessors, often along preexisting or self-generated outflow boundaries. They are usually smaller in scale than the TL/AS type but exhibit similar, although less robust, surface wind patterns.

Low-level jets often play a role in MCS formation. MCSs are found to occur most frequently in the evening and overnight (Maddox et al. 1979; Schumacher and Johnson 2006), which aligns well with climatology of the Great Plains LLJ. LLJs are prevalent in heavy precipitation cases, and often become atmospheric rivers in mid-latitudes when their source regions contain abundant moisture. Moore et al. (2003) create a storm-relative composite of numerous thermodynamic and kinematic fields within 21 heavy precipitation MCSs in an

attempt to define the environmental conditions and physical processes involved with these phenomena. A quasi-stationary frontal zone, in a region of low-level moisture convergence is found. The left exit region of a south-southwesterly LLJ is collocated with the composite MCS. Near surface winds are light and southeasterly, and veer considerably with height, indicating warm advection which is supported by other variable fields. A case study by Moore et al. (2012) details a series of MCSs which moved through Tennessee and caused extensive heavy rainfall and flooding during early May 2010. A strong southerly LLJ coupled with a persistent atmospheric river was a key mechanism for allowing the extreme rainfall observed.

In extreme situations, multiple MCSs can lead to more widespread flooding. Data from the Great Midwest Flood of 1993 are studied by Junker et al. (1999). A series of MCSs which occurred from June through September lead to this large-scale flood event. The scale and intensity of rainfall in these MCSs depended on many moisture-related variables, including: the magnitude of warm advection, the 1000-500 hPa mean relative humidity, the breath of the atmospheric river feeding northward into a surface boundary, and the strength of the low level moisture flux. Larger values for these moisture variables were correlated with higher rainfall totals.

In these studies, no single factor was found to solely predict the intensity of heavy precipitation, implying that the interactions between winds, moisture, and temperature are important. The datasets analyzed in this work focus only on moisture-related variables, with the goal of quantifying how well the evolution of one key variable for heavy precipitation (i.e. moisture) can predict the occurrence of heavy precipitation. Those wishing to forecast flash floods should keep this salient complexity in mind.

2.4 Using Anomalies as a Forecast Aid

Moisture anomalies have been used in multiple studies aimed toward forecasting applications. Junker et al. (2008) classify extreme wintertime precipitation events along the U.S. west coast using normalized anomalies of TPW derived from the NCEP model reanalysis. An understanding of the physical processes responsible for events is sought by binning precipitation amounts into light, moderate, and heavy categories. Heavy events show marked dissimilarities when compared to lighter events: the negative geopotential height anomalies are stronger, larger-scale, and more slowly moving for heavy events. TPW and low-level moisture flux are also anomalously high. Atmospheric rivers are observed with the three most extreme events. The implications for water availability in the West is noted by the authors. Northern California topography is complex, enhancing the importance of wind direction for creating heavy rain events.

Grumm and Hart (2001) present a method of analyzing standardized anomalies during the cold season to allow forecasters to predict extreme events. The anomalies derived are specific to both region and time of year. Model data from a number of extreme storms, including the historic 1993 Superstorm and the Cleveland Superbomb, are compared to a 30-year climatology of geopotential height, temperature, and sea-level pressure. Many of these record-breaking storms are highlighted by large deviations from normal. Grumm and Hart stress the usability of such a method, since it allows forecasters to intrinsically be given what is “normal” through use of deviations. Some criticisms include their subjective selection of cases, many of which only affected Pennsylvania, and which are of an unspecified “case type”. No null events, or “forecast busts”, were analyzed in detail.

Hart and Grumm (2001) examine 53 years of 12-hr NCEP reanalysis fields and determine the top 20 overall most anomalous events to strike the eastern U.S. in an attempt to objectively rank events. Top ten events are also listed for each specific variable analyzed. October through January are the months where it is most probable to have a “greater than four standard deviations from the norm” event, with April through September being the least probable to exceed this four standard deviation threshold. Graham and Grumm (2010) follow up this study with a similar methodology applied to the western United States. They also calculate a return period for each variable using the vertically summed anomalies for a variable and their frequency over the 59-year record.

Forsythe et al. (2012) use the NOAA operational TPWA product to examine the relationship between TPW and vertical clouds distribution. CloudSat and CALIPSO measurements are used to determine cloud structure. Three regions are examined in detail, with the hypothesis being confirmed for the northern Pacific and southern Mississippi Valley regions: cloud likelihood increases as TPW increases over 100% of normal. Over the eastern tropic Pacific, clouds grow vertically as TPW anomaly increases.

This research builds on the previous work summarized in this section. TPWA is not a standardized dataset, but in a similar manner to Grumm and Hart’s 2001 analysis, the TPWA product presents the user with output which includes information about both current observations and climatology. The non-Gaussian nature of TPWA creates some challenges when statistically examining the variable; however, multiple metrics can still be computed. Much of the previous literature uses anomalies for synoptic, cold-season events based on large-scale variables from models, such as 500 hPa height. With a higher spatial resolution dataset such as TPWA, it is possible to analyze more localized anomalies which often occur in water vapor fields and

precipitation accumulation. This makes the methodology used in this research useful for summer event forecasting, where mesoscale systems often cause localized heavy precipitation. Finally, it is important to note that steep terrain can cause heavy precipitation linked to high TPWA, but many of these orographically forced events are not included in this work due to difficulties that arise when attempting to verify summertime precipitation accumulation over mountains. Nevertheless, atmospheric rivers and moisture anomalies need to be considered in any future work over the Rocky Mountains, or any other steep mountain ranges.

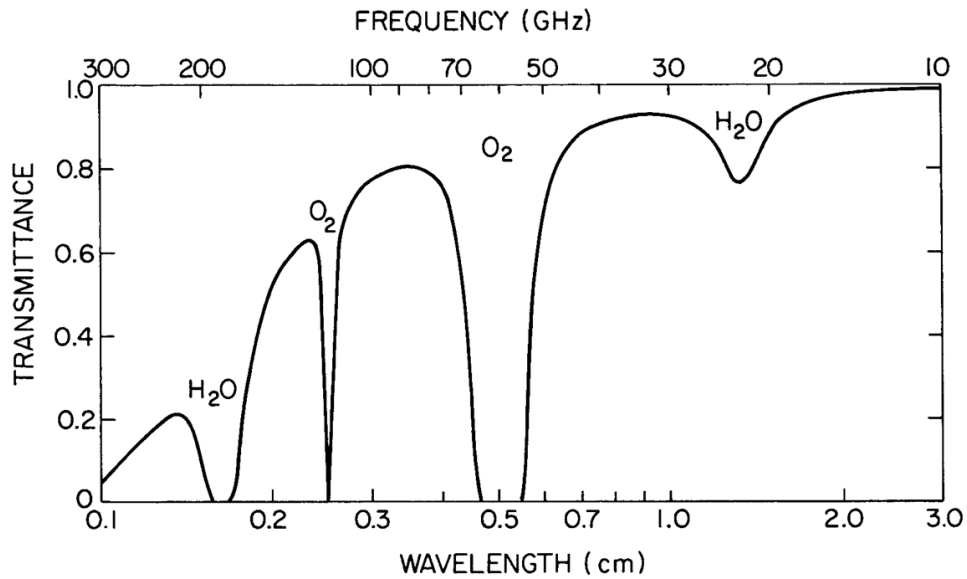


Figure 2.1: Transmittance for the passive microwave remote sensing region within the electromagnetic spectrum, 300–10 GHz. Labels show which atmospheric molecule is responsible for decreased transmittance. (reproduced from Kidder and Vonder Haar 1995)

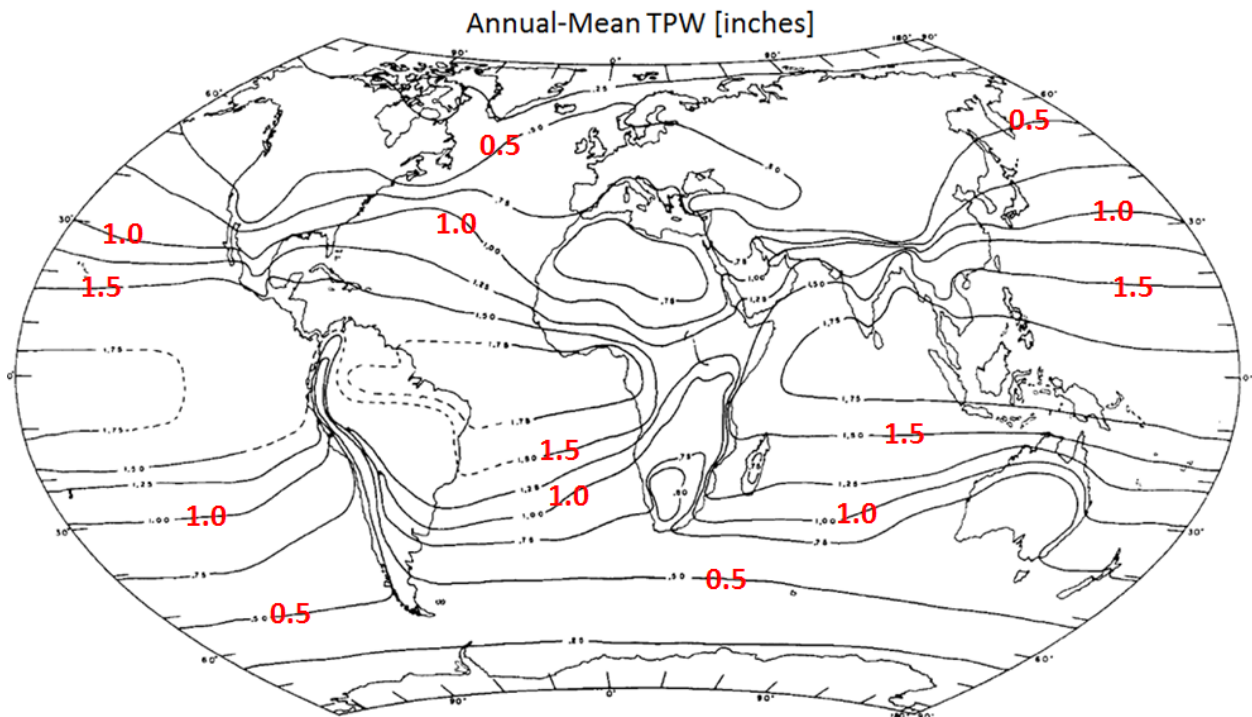


Figure 2.2: Annual mean TPW (inches) based on early radiosonde data. Contours every 0.25 inches. (reproduced from Tuller 1968)

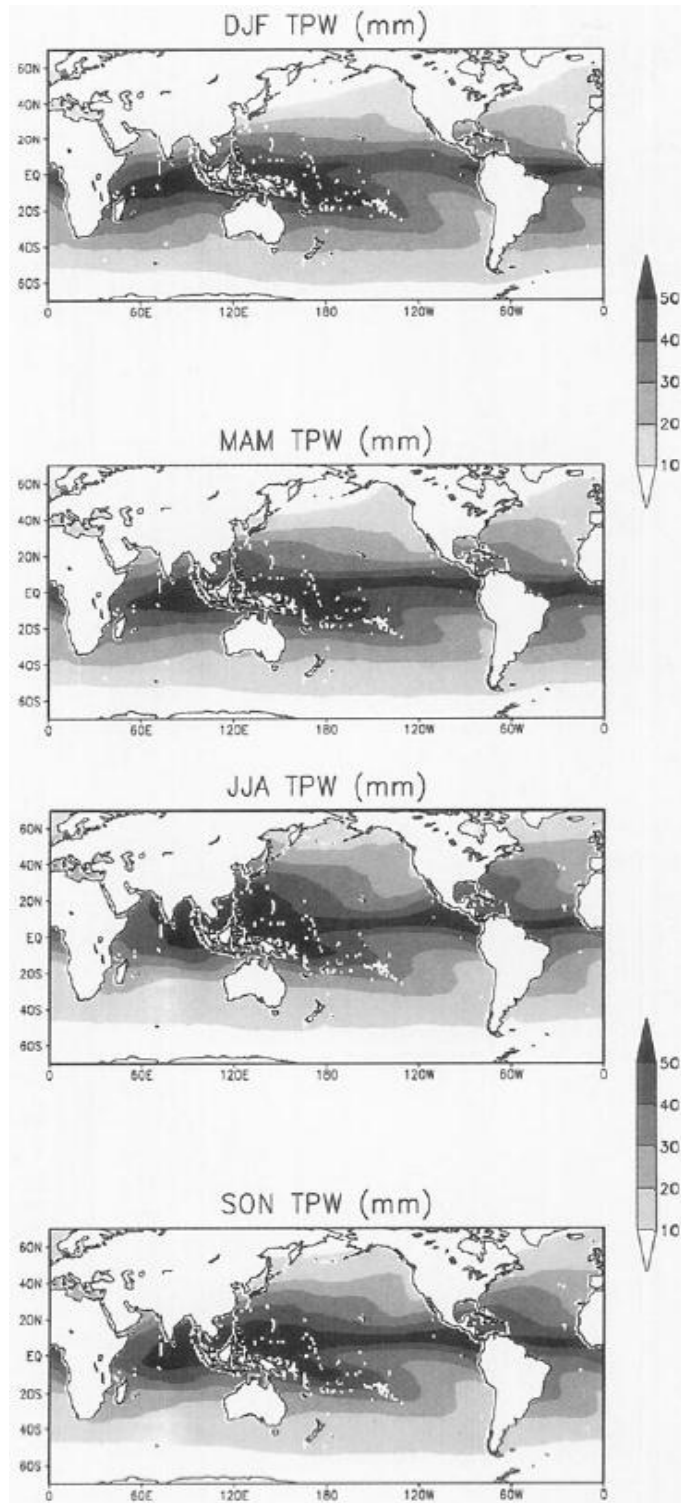


Figure 2.3: Seasonal mean TPW (mm) for DJF, MAM, JJA, and SON from 1987 to 1994. (reproduced from Ferraro et al. 1996)

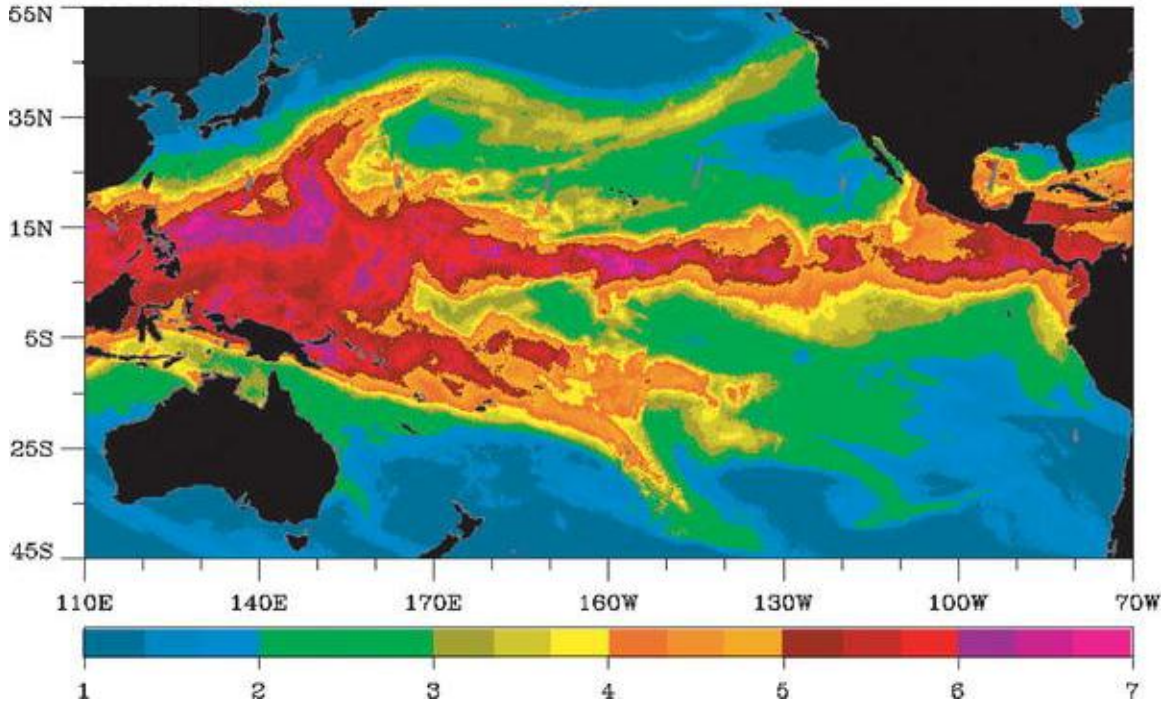


Figure 2.4: A well-defined atmospheric river as seen in TPW (cm) extending across much of the northern Pacific, and impacting North America. A southern branch of the Intertropical Convergence Zone (ITCZ) can also be seen in the southern Pacific. (reproduced from Bao et al. 2006)

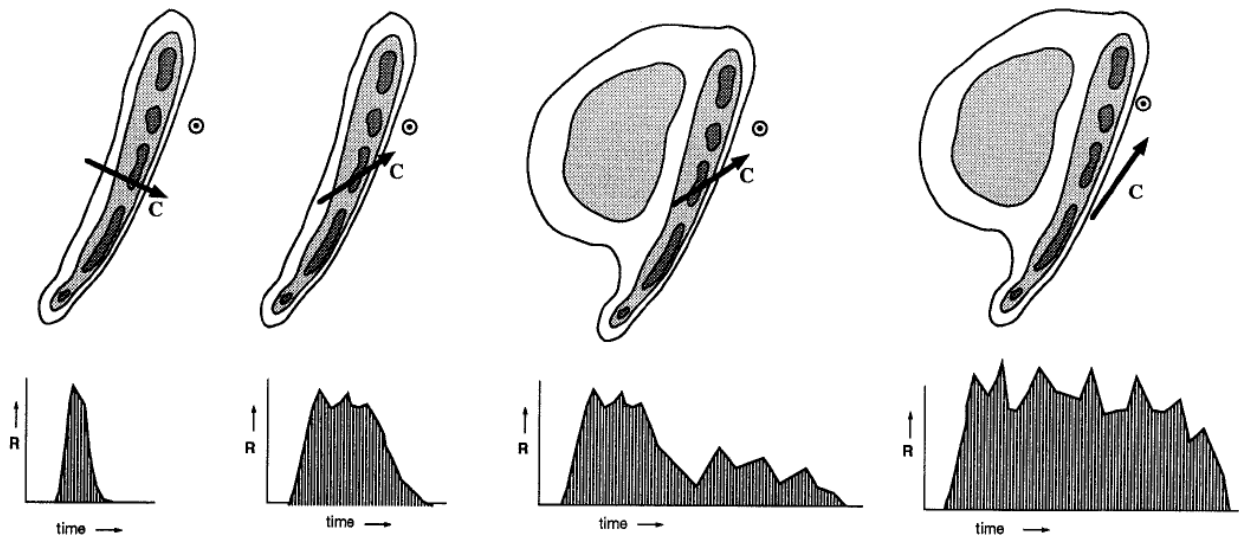
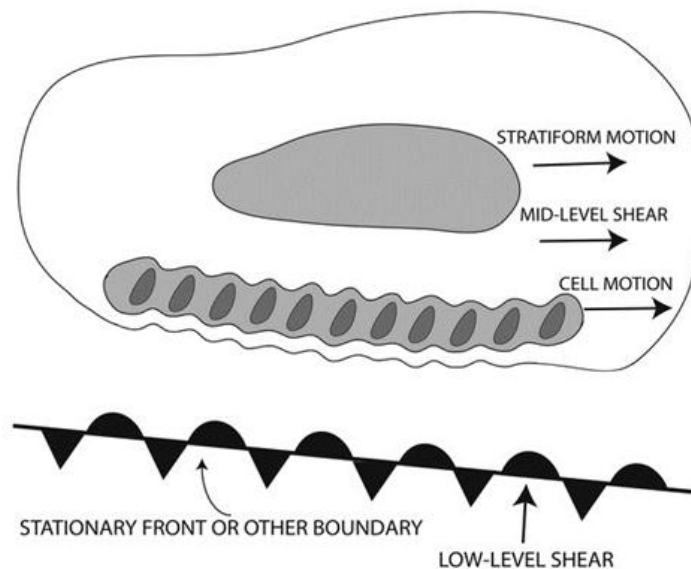


Figure 2.5: Reflectivity echoes from radar along with storm motion vector (top) and associated rainfall rate over time (bottom) at the point shown. The area beneath each curve is equal to total precipitation accumulation for the particular situation depicted. Units are arbitrary but consistent throughout the four situations. (reproduced from Doswell et al. 1996)

(a) TRAINING LINE -- ADJOINING STRATIFORM (TL/AS)



(b) BACKBUILDING / QUASI-STATIONARY (BB)

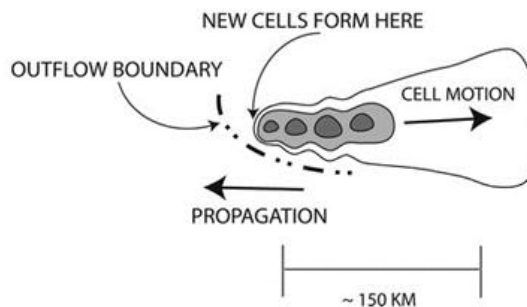


Figure 2.6: The radar-observed features of the two most commonly observed MCS structures found in heavy rain events, TL/AS (a) and BB (b). Reflectivity contours correspond to roughly 20, 40, and 50 dBZ. The length scale given is approximate. (reproduced from Schumacher and Johnson 2005)

3. INSTRUMENTATION AND DATA PRODUCTS

3.1 Blended TPW

This research uses the multisensor, satellite-based TPW product described in Kidder and Jones (2007). The product is mapped to a 16 km Mercator grid, and is produced hourly; however, there are gaps in the data due to the non-uniform distribution of satellite orbits (Fig. 3.1). The satellites utilized and the blending algorithms applied vary by surface type and location.

Over water, retrievals come from eight polar-orbiting, passive microwave instruments: either the Advanced Microwave Sounding Unit (AMSU-A) or the Special Sensor Microwave / Imager (SSM/I). Figure 3.1 shows the satellite names on which these eight instruments are mounted, as well as the orbits in which they fly. Input AMSU-A TPW retrievals are produced by the NOAA Microwave Surface Precipitation Products System (MSPPS) package using the 23.8- and 31.4-GHz channels (Weng et al. 2003; Ferraro et al. 2005). TPW values from MSPPS have a root-mean-squared error (RMSE) of 3.96 mm when compared to radiosondes. SSM/I retrievals are produced by the U.S. military's Fleet Numerical Meteorology and Oceanography Center (FNMOC) using the vertically polarized 19-, 22-, and 37-GHz channels (Ferraro et al. 1996). A histogram adjustment is employed to improve the continuity and aesthetics of the product, thus minimizing naturally-occurring "seams" in data due to intersensor differences (Kidder and Jones 2007). The adjustment matches the cumulative probability distribution functions for each scan position of each instrument to a chosen reference instrument (e.g. NOAA 17) to lessen differences.

The three most recent AMSU-A instruments aboard the Metop-A, NOAA 18, and NOAA 19 satellites allow for global, over-land retrievals via the Microwave Integrated Retrieval System

(MIRS) (Boukabara et al. 2010). These retrievals have a RMSE of 5.03 mm when compared to radiosondes. MIRS was utilized in the blended TPW product starting August 2010, nearly completing the global view of TPW in the blended TPW product.

A special set of TPW data inputs is utilized for the contiguous United States (CONUS). Over-water retrievals are still used where applicable. Additionally, three other sources attempt to populate the land surface with TPW. The primary over-land TPW data source is surface-based Global Positioning System (GPS) retrievals based on radio delay methods from the constellation of 24 GPS satellites. GPS radio signals from satellites are delayed in earth's atmosphere as they propagate. A dry atmosphere causes a set amount of delay, and water vapor adds to the delay. This small residual time delay can be measured by precise atomic clocks, and TPW can be calculated with an RMSE of 1.16 mm compared to radiosondes (Bevis et al. 1992; Duan et al. 1996; Meyer 2004; Rama Varma Raja et al. 2008). GPS TPW values are then extrapolated using a Barnes analysis (Barnes 1964; Koch et al. 1983) with user-defined parameters geared toward creating a smooth, high spatial coverage TPW field. There are currently over 500 NOAA/Earth System Research Lab (ESRL) receiving stations dispersed throughout CONUS (ESRL 2011). Geostationary Operational Environmental Satellite (GOES) East and GOES West Sounder retrievals are second in priority, and are used in any locations where GPS retrievals are not available. They are not as accurate or timely as GPS, and therefore are only used to fill in TPW when GPS is not available. The GPS data are also used preferentially because the GOES Sounders only retrieve TPW in cloud-free conditions, whereas GPS data can be used even with cloud cover. Data from the sounder are spatially coarsened to roughly 48 km² to reduce gaps between fields of view and to reduce noise in the retrievals. MIRS retrievals, analogous to those used for global land surfaces, are used if neither GPS nor GOES data is available.

An example blended TPW map from 0000 Coordinated Universal Time (UTC) 23 August 2011 is shown in Figure 3.2a. Note how the vast majority of the globe is covered in observations. The ice sheet in Greenland and the Antarctic continent lack observations, as neither MSPPS nor MIRS computes TPW over ice, and such regions are masked to avoid erroneous retrievals. Sometimes large, unphysical values do occur at the edge of sea ice, as seen around Antarctica. There are also gaps that arise periodically near the equator. These gaps appear because the suite of eight polar-orbiting, TPW-sensing satellites does not re-sample the entire earth within six hours. Meteorologically, there is a plume of high TPW over the south-central United States. A very well-defined tropical depression is located in the eastern Atlantic. Both the Andes and the Tibetan Plateau have extremely low TPW, due to their high elevations. Although the regions of high TPW, such as the tropics, do tend to receive more precipitation over the course of a year, Howell (2010) found that rainfall can occur at nearly any TPW value when taking a global perspective. This provides motivation for looking beyond TPW when seeking to develop a forecast aid.

Blended TPW is an operational product which is distributed hourly to the National Weather Service via the Advanced Weather Interactive Processing System (AWIPS) through NOAA's National Environmental Satellite, Data, and Information Service (NESDIS). The details of the product as listed in this section are accurate and current through the period of research, August 2010 through November 2011, but operational products often evolve. As older satellites are decommissioned, and new ones launched, future users of the data should carefully investigate any changes to the information listed here.

3.2 NVAP Climatology

The National Aeronautics and Space Administration Water Vapor Project (NVAP) is a daily, 1° resolution, global 4-layer PW (including TPW) dataset, which spans 12 years from 1988-1999. This research uses only the TPW. NVAP was created with TPW derived from radiosonde (land), SSM/I (ocean), and NOAA Tiros Operational Vertical Sounder (TOVS; ocean and land) (Randel et al. 1996).

Radiosonde measurements have historically been the basis for water vapor statistics (Oort 1983). NVAP incorporates a statistically analyzed, quality controlled, global set of upper-air soundings as described by Ross and Elliott (1996). Sounding temperatures that do not pass within 4 standard deviations of the mean at the required atmospheric pressure levels are discarded if they do not reach to 700 hPa. Good data are retained for the lower atmosphere if the failed check occurs at a level higher-up in the atmosphere, above the 700 hPa level. This allows the lower levels, which contain the bulk of the water vapor, to be retained in NVAP, even when part of a profile is missing. Radiosondes are given the highest confidence in creating the final climatology.

SSM/I data from DMSP F-series satellites were input using a physical retrieval scheme described by Greenwald et al. (1993), with requisite SSTs taken from an NCEP product on a 2° x 2° global grid (Reynolds 1988). SSM/I retrievals include a 0.5° land mask, yet sea ice, small islands, and heavy precipitation can still lead to erroneous values.

The TOVS instrument package orbited aboard the NOAA-series of satellites, and included three cross-track instruments which were used in concert to retrieve TPW (Smith et al. 1979; Kidder and Vonder Haar 1995). TOVS retrievals are given a lower confidence than SSM/I

or radiosondes due to a dry bias in thick clouds (Wu et al. 1993) and a wet-bias in regions of large-scale subsidence (Stephens et al. 1994).

The NVAP dataset has undergone extensive quality control (QC) by using automatic detection and manual methods. QC challenges are listed by the principal investigators in Vonder Haar et al. (2003). The aforementioned report also notes the time-dependent biases in the dataset.

Figure 3.3 shows an example of NVAP daily-mean TPW from 13 July 1999. One can pick out multiple atmospheric rivers over the ocean basins, most notably in the Pacific. High values of TPWA are located near the Kuroshio Current in the western Pacific. The poles are driest, with the south pole having the lowest TPW during austral winter. The Intertropical Convergence Zone (ITCZ) also has elevated TPW due to evaporation from the tropical ocean regions, with global circulations serving to further enhance TPW in the ITCZ (Marshall and Plumb 2008).

3.3 Total Precipitable Water Anomaly

The Total Precipitable Water Anomaly (TPWA) data product is created by dividing the blended TPW product (Kidder and Jones 2007) by the 1988-1999 NVAP climatology (Randel et al. 1996). There are 52 weekly mean fields used as normal from NVAP. These means are stationary, and change per week, but are not recomputed as a moving mean for each day. The blended TPW value on a given day is divided by the climatological “normal” value for that week, and this number is then multiplied by 100% to give a “percent of normal” TPW. This is the operational method in use at NOAA to calculate anomalies. The data are gridded to the same 16 km Mercator projection as blended TPW. The dataset is often referred to as “Percent of Normal TPW”. The percent of normal product was developed at CIRA for research purposes, but has proven useful for tracking atmospheric rivers, return flow of moisture from the Gulf of

Mexico, and abnormally dry conditions associated with fire danger. TPWA is a NOAA NESDIS operational product, and is updated hourly.

The product is especially robust in mid-latitudes, where it shows a large range. In the tropics, even hurricanes do not generate values greater than 200% since the climatological state is already extremely moist. These observations point out that forecast rules and statistics are regionally meaningful for TPW, but caution must be taken when transferring across vastly different climate regimes.

An example of the TPWA product is shown for 0000 UTC 23 August 2011 in Figure 3.2b. Abnormally moist areas are shaded in blue increasing to green, with yellow being reserved for anomalies surpassing 200%. The color scheme is chosen to highlight the above normal regions. Dry regions below 100% of normal TPW are shaded in increasingly dark shades of brown. Dry air masses are in place over both the Andes and the Tibetan Plateau, leading to lower than average TPW. Notice how the tropics have the smallest range of values due to their moist background state. A tropical depression sits in the eastern Atlantic, and even it has difficulty producing an atmosphere more moist than 150% of normal. Regions covered by ice, such as Greenland and Antarctica are data void, with the edges of these features producing extremely high, spurious TPWA amounts. Many atmospheric rivers can be seen in the winter hemisphere, which is the southern hemisphere in this example. A couple atmospheric rivers are also seen in the northern hemisphere: two in the Pacific and one over the Great Plains.

The TPWA product was originally created to highlight and quantify atmospheric moisture features for the forecaster. Forecasters in the NWS currently use the product for checking atmospheric water vapor availability to assist in making precipitation forecasts and fire-weather decisions (R. Cox, NWS Science Operations Officer, 2012, personal communication).

This satellite product supplements hourly surface dew point observations taken at many ground observing stations.

3.4 Stage IV Precipitation

NCEP's Stage IV precipitation analysis, which is a mosaicked national multi-sensor precipitation analysis, is also used in this study. The product has approximately 4 km resolution, covers CONUS, and is available hourly, with both 6-hour and 24-hour composites available. The primary data input is calculated precipitation accumulation from the approximately 140 CONUS Weather Surveillance Radar-1988 Doppler (WSR-88D) Precipitation Processing Systems (PPS). Additional inputs include Automated Surface Observing System (ASOS) Meteorological Aerodrome Reports (METAR) and Hydrometeorological Automated Data System (HADS) gauge reports (Lin and Mitchell 2005). The 6-hourly and 24-hourly Stage IV precipitation products benefit from manual quality control by the 12 River Forecast Centers (RFCs). This research uses the 6-hourly product.

Fulton et al. (1998) detail the algorithms used in the PPS. The PPS is a set of algorithms that operates in sequence using reflectivity factor (hereafter simply called "reflectivity") data as the fundamental input. Reflectivity data are collected with 0.5 dBZ precision continuously in 360° sweeps to 230 km with a resolution of 1° by 1.0 km. Temporal sampling is between 5 and 10 minutes, depending on the volume scan pattern. PPS automatically detects when measurable rainfall initiates, based on reflectivity thresholds, and begins calculating precipitation accumulation at that time. Reflectivity data from the lowest 4 scans angles can be used to calculate rainfall. The angle closest to ground level is used, unless terrain interferes, in which case the next lowest scan angle is used. Bright band contamination, partial beam blockage, and ground clutter factors are addressed by attempting to avoid including the bright band by choice

of scan angle, using offsets based on percent of beam blockage, and testing for anomalous propagation due to tight temperature or moisture gradients.

A standard, empirically-derived Z-R power law relationship is employed to convert reflectivity to rain rate once the reflectivity retrieval is made. The default equation is

$$Z = 300R^{1.4} ,$$

where Z has units of $\text{mm}^6 \text{m}^{-3}$ and R is in mm h^{-1} . Some locations in more tropical regions use a modified form. The quality control for this step includes removing high values associated with hail cores and replacing them with more realistic values based on surrounding retrievals, a time continuity check, and a range degradation correction.

Rainfall rate is then integrated over the time from scan-to-scan to produce a precipitation accumulation, with missing scans being filled by linear extrapolation of up to 30 min using the previous two time steps. Outliers are removed based on a threshold and nearest-neighbor check.

Finally, rainfall accumulations are tested against current ground observations. A “mean field” bias adjustment is applied to the entire radar’s domain. This bias is determined using a discrete Kalman filter (Ahnert et al. 1983) which gives the statistical significance of the differences in paired gauge-radar observations. If there is large mean square error (i.e. wide scatter) between gauge-radar pairs, a small mean field bias is applied, and vice versa. As one can imagine, a stratiform event with uniform overestimation by the radar will result in a relatively large mean bias correction so that radar values approach observations. A severe weather event where only a few pairs report large differences will result in less of a mean field bias correction. The result of the PPS is a Digital Precipitation Array, or “Stage I” rainfall accumulation map, for an individual radar site, among other products.

The next step is the assimilation of approximately 1450 ASOS hourly and any of the available 14000 HADS hourly precipitation reports. An optimal estimation scheme is then used, given partial coverage of both radar and gauge observations, to create the Stage II product (Baldwin and Mitchell 1997). Stage III is created by the RFCs and combines all Stage II products within their basin using a multisensor precipitation estimator. The Stage III product is now called the Regional Multi-Sensor Precipitation Analysis (RMPA). The final step is sending the RMPAs to NCEP where the 6-hourly and 24-hourly data undergo manual quality control and are quilted into a national Stage IV map.

Figure 3.4 depicts an example Stage IV Precipitation product from 1200 UTC 01 May 2010. The data are mapped to a 4 km Mercator projection. Extreme rainfall amounts occurred during this prolonged heavy precipitation event, which was caused by two quasi-stationary linear MCSs (Moore et al. 2012). Locations near Memphis, Tennessee have received in excess of 200 mm of precipitation for the time period shown, as seen by the red and purple fill in the product.

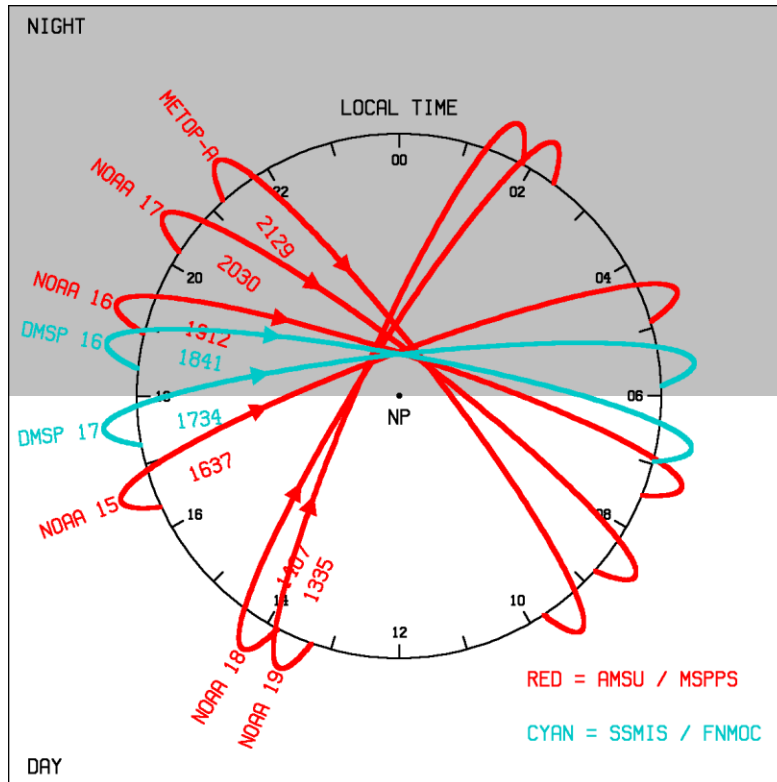


Figure 3.1: Names, orbits, and ascending node local equatorial crossing times for the polar-orbiting satellites included in the blended TPW product. Satellites with the AMSU-A instrument are shown in red, and those with the SSM/I are shown in cyan.

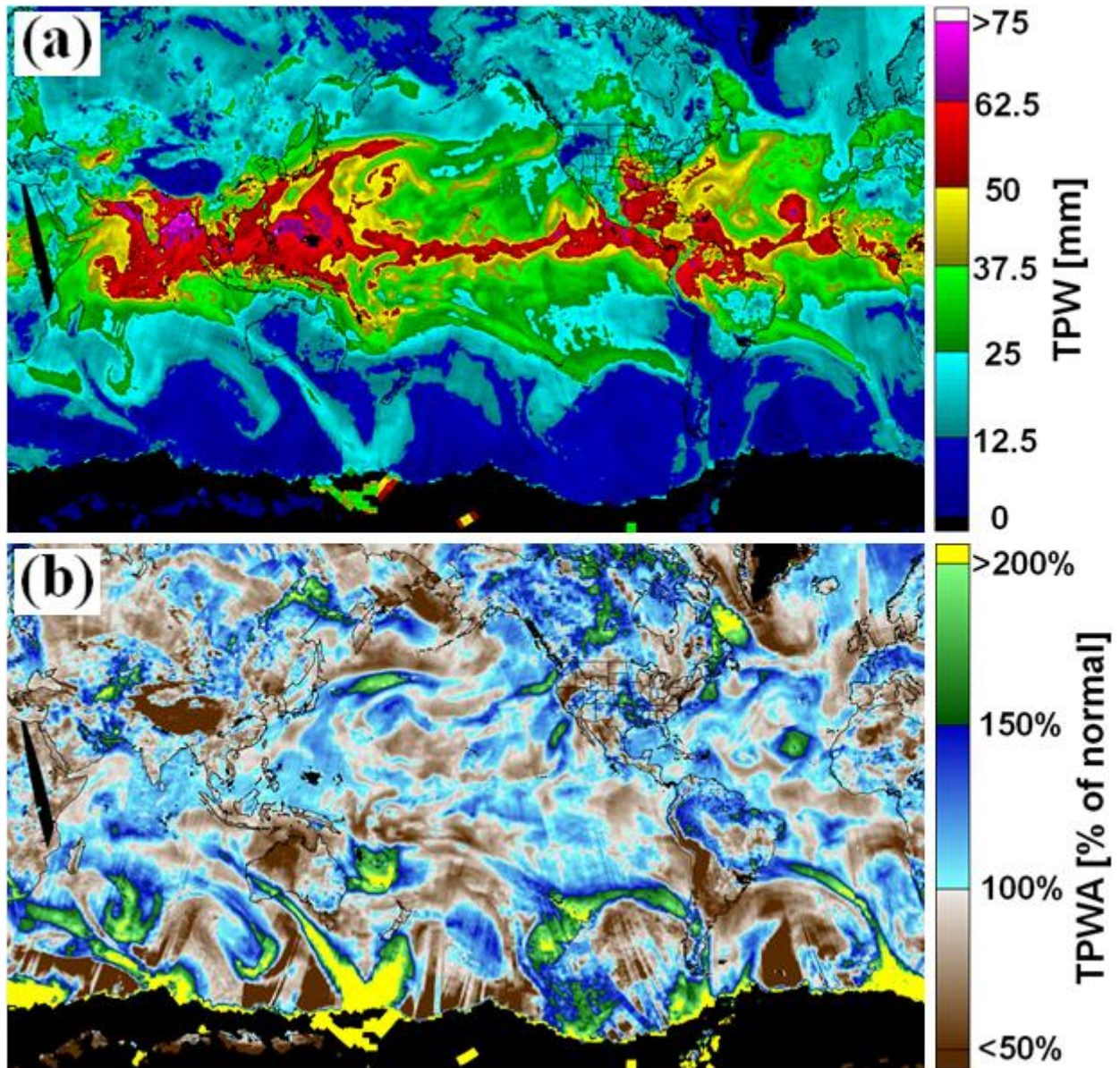


Figure 3.2: Example blended TPW product (a) and the corresponding TPWA product (b) for 0000 UTC 23 August 2011. TPW has units of millimeters and TPWA ranges from <50% to >200% of normal.

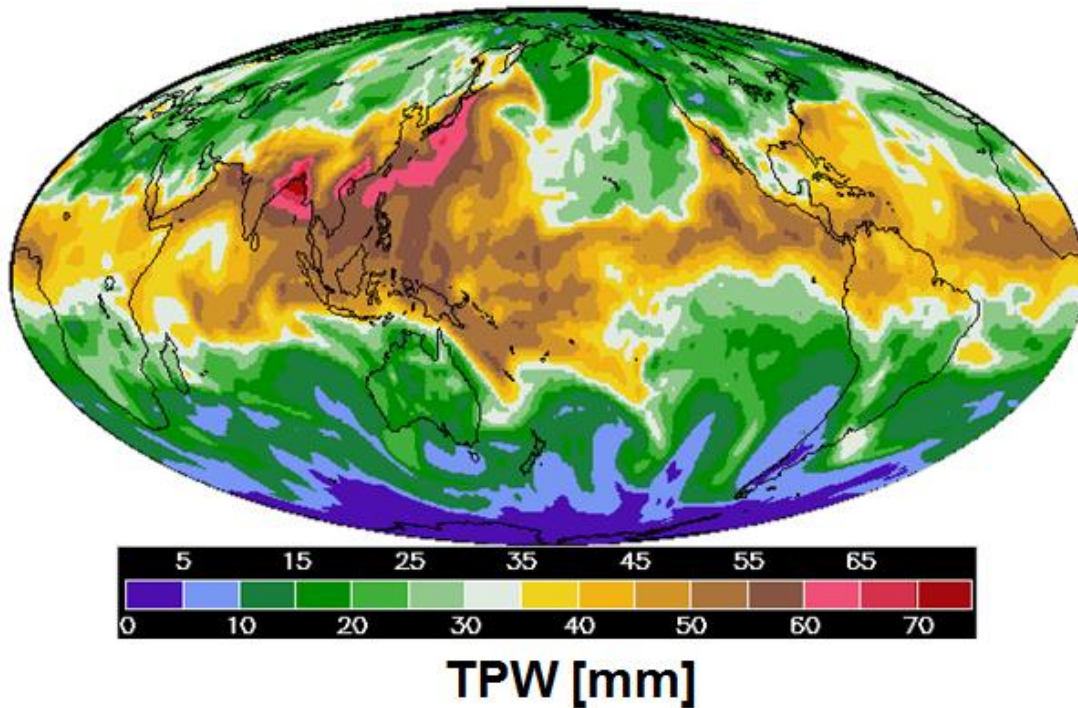


Figure 3.3: Example daily-mean NVAP TPW (mm) for 13 July 1999.

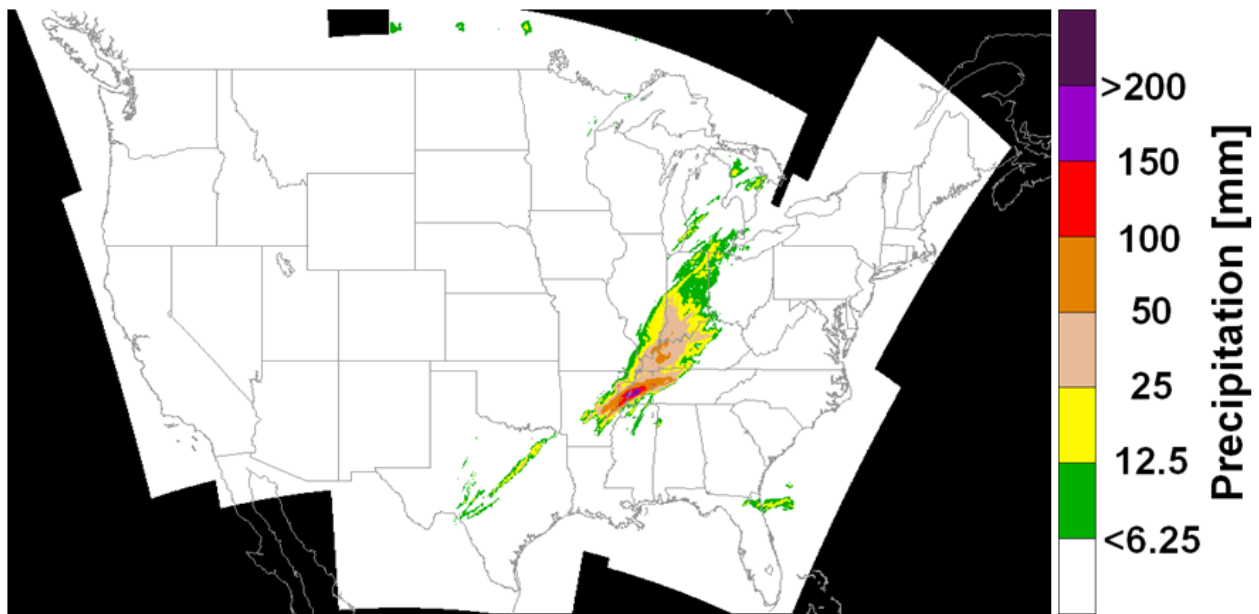


Figure 3.4: Example Stage IV Precipitation accumulation for the six hours ending 1200 UTC 01 May 2010 showing high rainfall accumulations in southwestern Tennessee. The black regions are areas not included in the product. White areas are places that received less than 6.25 mm of precipitation in the 06–12 UTC timeframe.

4. METHODOLOGY

4.1 Heavy Precipitation Event Analysis

The term “heavy precipitation event” must be quantified in order to test the hypothesis that TPWA will be positive and increasing in time preceding such an event. For the purposes of this study, a “heavy precipitation event” is one in which the precipitation amount for the 6-hour duration, 50-year return period is exceeded. This threshold is commonly referred to as the 6-hour, 50-year recurrence interval. Mathematical functions are used to estimate the amount of precipitation that has a 2% probability of occurring at a given location in a given year. The “event time” is defined as the 6-hour period where precipitation accumulation exceeded the 50-year precipitation amount. Regions more prone to heavy rainfall require a larger amount of precipitation to surpass the threshold. Hershfield (1961) details his methods for estimating these thresholds in his seminal paper to the Weather Bureau (presently, the NWS). The 6-hour, 50-year recurrence map is shown in Figure 4.1. Gulf Coast state coastlines have the highest precipitation amounts, and values generally decrease poleward. Hershfield recurrence intervals are still used as a primary source for return periods in many locations despite their coarse resolution, and were for this reason used in this study.

A list of heavy precipitation events was created by examining 6-hourly Stage IV Precipitation data and comparing accumulations to the Hershfield recurrence interval amounts. Stevenson and Schumacher (2012) used the Automated Geospatial Watershed Assessment Tool to access a digital version of the recurrence maps made by Hershfield. The spatial resolution of the Stage IV Precipitation data were then coarsened to an 8.25 km grid to help eliminate the identification of spurious events. Legitimate, finer-than-8.25 km spatial scale events may have been removed by this process. Intense, larger-scale events can cause tens of 8.25 km gridpoints

to exceed the 50-year recurrence interval. If an exceeding gridpoint lies within 100 km of another exceeding gridpoint, the second point was ignored and counted as the same event based on the primary gridpoint. Precedence was given to gridpoints in the northwest due to the algorithm's search process, which identifies gridpoints north to south, and west to east. Gridpoints outside a primary gridpoint's 100-km radius were treated as separate events. 107 events were identified using the methodology described. Of these 107 events, 84 were used after applying quality control (Table 4.1), as discussed in section 4.4.

The coarse resolution of the Hershfield recurrence intervals cause events to preferentially lie near the southern edge of the interval bands. Figure 4.2 shows the locations of all 84 events that were tested for the study's duration. Over 80% of events lie in the southern half of their respective recurrence interval band. Although some of this tendency may be explained by chance due to the limited sample size of 84, it is undoubtedly compounded by the coarse recurrence interval resolution. Increasing the Hershfield recurrence interval data resolution by using a simple linear interpolation could help increase event identification in the northern portion of the bands in future work.

The definition of a heavy precipitation event used in this research does not explicitly exclude winter precipitation events, and extreme winter events could theoretically be identified by this method. Nevertheless, climatology suggests that the largest precipitation accumulations for 6-hour timeframes occur during the warm season via convective rainfall in the central and eastern United States. Meteorological phenomena such as MCSs, land-falling tropical cyclones, slow-moving supercells, and stationary fronts are the primary causes of exceeding the 6-hour, 50-year recurrence interval. The results of this study are therefore most directly applicable to warm season events, roughly from April to September in the United States.

4.2 Domain Considerations

It is important to consider the size of a domain chosen to represent a statistic such as area-mean TPWA. Results are a function of event domain size. In the extreme, a global mean would yield little about a particular storm event, whereas a point value would tell one nothing about the surrounding environment. Multiple event domain sizes were tested: 160 x 160 km (roughly 1.9° longitude x 1.5° latitude), 200 x 200 km (roughly 2.5° x 1.9°), and 250 x 250 km (roughly 3.0° x 2.3°). The exact size in degrees varies with latitude, since the earth's surface is spherical. These are approximately 26000, 43000, and 64000 km² respectively. All three of these domain sizes showed a signal of positive and increasing TPWA preceding an event (Fig. 4.5), suggesting that none of the domain sizes were unreasonable. As domain size increases, the positive TPWA signal weakens slightly, as more environmental values are included in the area-mean. The 200 km domain was ultimately chosen for further analysis, since it contains over 323 unique TPWA data points, is large enough to be representative of the mesoscale environment at the location, yet is not too large to suppress TPWA variability. Future work may supplement the following analysis by including results based on alternate domain sizes.

A domain centered at the exceeding gridpoint was chosen to capture the evolution of TPWA in the environment. A centered domain allows for the sensing of moisture flux from any direction. Additionally, the domain is stationary/fixed throughout an event. A fixed domain is more feasible to implement operationally. No additional data containing ambient wind patterns or climatology are necessary in order to make a prediction for a location of interest. This may be a hindrance for those looking to include the forecast skill that model data would potentially provide, but a simple stationary domain is an advantage for users in remote locations where little computing power and/or supplementary data are available. This research is targeted toward the

remote user, and aims to be a useful, impromptu calculation that serves as a quick aid for forecasters, with little background knowledge necessary. Another option for future study would be to advect the domain through time using model wind forecasts so that it matched the area of interest during the time period where the heavy rain recurrence interval was exceeded. This alternate method would be more storm-centric, perhaps providing additional forecast skill.

The 84 heavy precipitation events and 12 forecasting locations chosen for this study are located in the central and eastern United States. Areas of exceptionally complex terrain, common in the western U.S., were intentionally avoided to reduce underestimated precipitation values that commonly occur in extreme terrain. TPWA is a quasi-global product, so the astute global user may wonder the extent to which the results are transferrable or generalizable. To fully answer this question, similar studies would have to be done over the oceans, and other landmasses. The U.S. is unique in that comparison data (e.g. Stage IV Precipitation) are regularly collected, readily available, and often quality controlled in some manner. Doing a similar study over remote regions would require more effort and likely result in fewer verification data, but this does not make such an effort impossible. Visual inspection of global TPWA maps show that mid-latitude locations would likely have similar behavior to the United States. Tropical locations have a moist climatology, and thus have lower anomalies, which would likely lead to lower area-mean signals in TPWA. High latitude regions add complexity due to ice and sea ice.

A final consideration is the data input differences between the U.S., global land, and the oceans. MIRS retrievals rarely contribute to U.S. anomalies via the blended TPW product. Although both MIRS and GPS retrievals determine TPW, there may be systematic biases between the two schemes. Users applying the results of this study outside of the U.S. should keep this caveat in mind.

4.3 Temporal Considerations

The TPWA product used began being computed February 2006, and data as recent as November 2011 were available for this study. Beginning at 0000 UTC 20 August 2010, MIRS retrievals were added to the TPWA product. The addition of MIRS made it possible to retrieve TPWA over global land surfaces. Previously, only U.S. land areas had TPWA computed from the GPS and GOES water vapor retrievals. August 2010 through November 2011 was chosen for the study period in which heavy precipitation events were analyzed statistically in order to ensure consistency. Land surfaces for the study period include MIRS retrievals, making late 2010 and 2011 the most globally generalizable and representative for analyzing TPWA, since TPWA product inputs are most similar during this study period.

The area-mean TPWA was computed from 72 hours (3 days) before until 48 hours (2 days) afterward for each of the 84 events, spanning 21 six-hourly timesteps. An identical area-mean Stage IV Precipitation computation was performed. Both TPWA and Stage IV Precipitation area-mean time series were plotted (Fig. 4.3). Additionally, spatial TPWA data for each event domain were extracted and plotted for each timestep to examine the zonal and meridional structure of TPWA (Fig. 4.4) in the event domain. Events which crossed the TPWA threshold over multiple 6-hour periods were treated as separate events, even if they were forced by a single weather system. The focus for this study is on the 24 hours immediately preceding an event, since a primary objective is to quantify TPWA evolution to aid in forecasting. Nevertheless, the time well-beforehand and afterward was included to observe the temporal context of TPWA evolution.

4.4 Data Quality Assurance

Stage IV Precipitation is a complete, quality controlled dataset with no egregious errors that required the author's attention. It was used "as is" from NCEP. TPWA is much more problematic, and required manual quality control.

Heavy precipitation events were excluded from statistical analysis if they were missing TPWA data for more than three 6-hour timesteps, had more than two consecutive missing timesteps, or were missing any data within 12 hours of the event time. Events were not counted if any of these three critical tests did not pass. Data for the most recent (relative to time being considered) 6-hour period available were used to fill-in other data voids which did not cross any of these critical thresholds.

Missing data points are present in many TPWA data files. Orbits do not completely re-sample the globe every 6 hours leaving small data gaps (see Fig. 3.2, eastern Africa). Extreme precipitation with rainfall rates of over 2-inches per hour also can cause unusable microwave retrievals which are masked as missing data. GPS retrievals over the U.S. help offset this drawback, leading to less than 8% of the 84 events having any precipitation screening at the event time. Nevertheless, as a secondary check, timesteps in which over 25% of the 323 TPWA data points are missing are marked as completely missing in the area-mean TPWA calculation in order to prevent averaging of a significantly smaller number of non-representative points in a domain, which could falsely skew the average for that timestep. Such missing timesteps are not included when calculating the event-average TPWA evolution.

4.5 Forecasting With TPWA

Investigating the extent to which the TPWA data product can be used as a forecast aid requires the information gleaned from the statistical analysis of heavy precipitation events to be turned into a forecasting methodology. Average, upper quartile, and lower quartile area-mean TPWA values for the -18 to -6 hour range were used in the development of multiple thresholds in order to quantitatively determine the connection between rising, anomalously-positive TPWA and precipitation accumulation.

Twelve “forecasting locations” were chosen across the United States. Locations were chosen to span the central and eastern U.S. with approximately equal spacing (Fig. 4.6). The domain size of the 12 forecast locations match the domain size of TPWA heavy precipitation events, namely, 200 x 200 km. This allows for area-mean precipitation accumulation comparison. Area-mean TPWA is computed alongside area-mean precipitation for the twelve forecasting domains for the entire year of 2011. The result is two time series for each of the 12 locations. The time series are 1460 timesteps in length, which is a function of the 365 days in a year and the four 6-hourly time periods per day. The year 2011 was chosen to correspond closely with the study period used for heavy precipitation events. It should be mentioned that numerous data gaps in TPWA caused the usable length of both time series to be 1136 timesteps.

The two time series for each forecasting location were examined using TPWA thresholds to explore the relationship between TPWA and heavy precipitation. An algorithm moves forward through the coincident time series attempting to predict a heavy precipitation event based solely on TPWA evolution. When the currently set TPWA threshold is exceeded, a “forecast” is made, and the algorithm analyzes the future timesteps and records the amount of precipitation that accumulates after the forecast, comparing it to a user-set precipitation threshold. In a real-time

forecasting situation, it would be impossible to know the result of a forecast until hours later, but using past data allows this computation to be done immediately. Specific algorithm settings are modified to determine the effectiveness of various forecast threshold combinations. There are five parameters tested which give a myriad of results based on every possible combination. The variables include: threshold adherence, threshold length, threshold values, precipitation accumulation timeframe, and forecast location. Each is described in detail below, and Figure 4.7 depicts this information visually. Figure captions in the relevant figures state which threshold is being used.

A. Threshold Adherence (strict, moderate, loose)

Threshold adherence refers to how closely the threshold adheres to the information gained from the statistical analysis of the 84 heavy precipitation events. A strict adherence requires that TPWA be increasing in time, and also be greater than the threshold values for the entire threshold length. A moderate adherence requires that TPWA be increasing, but only needs to be greater than the threshold value at the current timestep. A loose adherence requires that TPWA only must be greater than the threshold value at the current timestep, and may be increasing or decreasing beforehand. As one progresses from strict to loose adherence, the sophistication of the algorithm decreases, allowing for easier computation. All results shown use the moderate threshold adherence. The strict and loose adherences were tested, but the loose adherence leads to severe over-forecasting, and the strict adherence leads to under-forecasting. For this reason all results shown are based on the moderate adherence.

B. Threshold Length (6 hour, 12 hour, or 18 hour)

Threshold length refers to how many previous timesteps, in addition to the current timestep, are being considered. This variable establishes the time period over which one desires TPWA to be increasing before triggering a forecast to be made. A threshold length of 6 hours requires only that the timestep immediately preceding the current time must have a TPWA less than the current time. A threshold length of 12 hours requires TPWA to be increasing over the two immediately preceding timesteps. The latter is a more restrictive case, and lowers the number of forecasts made. 18 hours was also examined, but results are not shown. The 18 hour threshold length was found to produce very few forecasts, and therefore could not be verified well. The focus in the results section is on the 6 and 12 hour threshold lengths.

C. Threshold Values (lower quartile, average, upper quartile)

Threshold values are the TPWA values which the algorithm must surpass to produce a forecast. There are values specified for each of the following: the lower quartile, the average (arithmetic mean), and the upper quartile. The upper quartile results are not shown since few forecasts are made over the 6 months examined when requiring such a high TPWA threshold. Results focus on the average and lower quartile threshold values.

D. Precipitation Accumulation Timeframe (6 or 12 hour)

The two precipitation accumulation timeframes correspond to the amount of time over which area-mean precipitation is summed over to check against the precipitation threshold. The algorithm checks to see the total precipitation which occurred during the timeframe. A “hit” is recorded if the amount is greater than what is set for the precipitation threshold (explained below), and a “miss” recorded if the amount is less than the precipitation threshold. Although

both were tested, the results from 6 hour accumulation timeframe outperform the 12 hour timeframe, and only the 6 hour accumulation timeframe results are shown.

E. Forecast Location (12 distinct locations)

Each location has a pair of time series over which to use the various thresholds. The individual forecast locations are referred to by the two-letter state abbreviation in which their center point lies.

Each variation of the forecasting algorithm is run over each forecasting location's TPWA time series and precipitation time series. The algorithm begins at 0000 UTC 1 April 2011 and runs through 0000 UTC 1 October 2011 for each variation: a six month period. When moving through the time series, it assumes the current time is "-6 hours", i.e. a precipitation event could occur at any time. If the currently set TPWA threshold is crossed, it checks the next time step to see if a precipitation event of sufficient magnitude is detected. Precipitation thresholds of 6, 9, and 18 mm were used. The 18 mm precipitation threshold corresponds to the average value observed during the 84 heavy precipitation events analyzed, but was crossed less than 10 times total at all forecast locations; therefore, the algorithm variations requiring this threshold are not included in the results section.

Algorithm forecasting skill is verified using standard dichotomous contingency table statistics. Figure 4.8 shows the table used for this research. The rows indicate whether an event was forecast (yes or no). The columns indicate whether an event was observed (yes or no). Summing the rows or columns gives a total for the respective row or column. A "hit" occurs when an observed event was correctly forecast, and a "miss" occurs if an observed event was forecast not to occur. A "false alarm" lets the tester know that a yes forecast was made and no

event was observed, whereas a “correct negative” indicates that a no forecast was made and no event was observed. A perfect forecast system would only produce hits and correct negatives. The total forecasts and total observed events are circled in grey in Figure 4.8, because these are explicitly shown in the results section.

It is necessary to define what a “forecast” is and what an “observed” event is before using the contingency table for a specific application. When the TPWA threshold described previously in this section is exceeded for a timestep, a forecast is made. An observed event is defined as area-mean precipitation crossing the currently set precipitation accumulation threshold, e.g. 6, 9, or 18 mm. Hits occur when the precipitation threshold is crossed over the precipitation accumulation timeframe (explained above). Analogously, a miss is counted if a TPWA threshold was not crossed immediately before sufficient precipitation accumulation.

There are many different metrics which can be derived from the various combinations on the contingency table (Wilks 2011). This research examines two metrics which are used widely in forecasting verification: probability of detection (POD) and false alarm ratio (FAR). POD and FAR are defined as follows:

$$POD = \frac{hits}{(hits+misses)} * 100\%$$

$$FAR = \frac{hits}{(hits+false\ alarms)} * 100\% .$$

POD lets the forecaster know the percentage of observed events which are properly forecast, whereas FAR allows the forecaster to know how often the forecast tool “busts”, i.e. claims an event will happen and it does not happen. These two metrics should always be used in concert with each other because neither gives a complete picture alone. For example, POD can easily reach 100% by making a forecast at all times, ensuring all observed events had a forecast

made. This is not practical, because this would obliterate the forecaster's trust in the tool. This trivial method will lead to an extreme number of false alarms, greater than 99%, therefore letting the forecaster know the tool is not performing well. If taken to the other extreme, a forecast tool may only predict the most extreme events, creating a very low FAR by "playing it safe". This method would result in a low POD. In summary, high percentage POD along with low percentage FAR indicate high forecasting skill for a forecasting algorithm.

The NWS sets yearly POD and FAR goals for warnings they issue: tornado, flash flood, winter storm, etc. They use these metrics as a way to judge forecast performance. It is difficult to make an "apples to apples" comparison between NWS warning goals and the results of this study, since the definition for "forecast" and "observed" event vary dramatically, and depend heavily on many choices set by the tester. Additionally, these NWS POD and FAR goals are for warnings, which have lead times shorter than the forecasts being tested in this research. Nevertheless, they give a sense for what values are reasonable in the operational, "rare event" realm. The U.S. NWS Central Region goals for tornado warning verification in 2012 were >72% POD, and <72% FAR (J. Griffith, NWS Warning Coordination Meteorologist, 2012, personal communication). The 2012 flash flooding goal for POD was >74%, with no set goal for FAR.

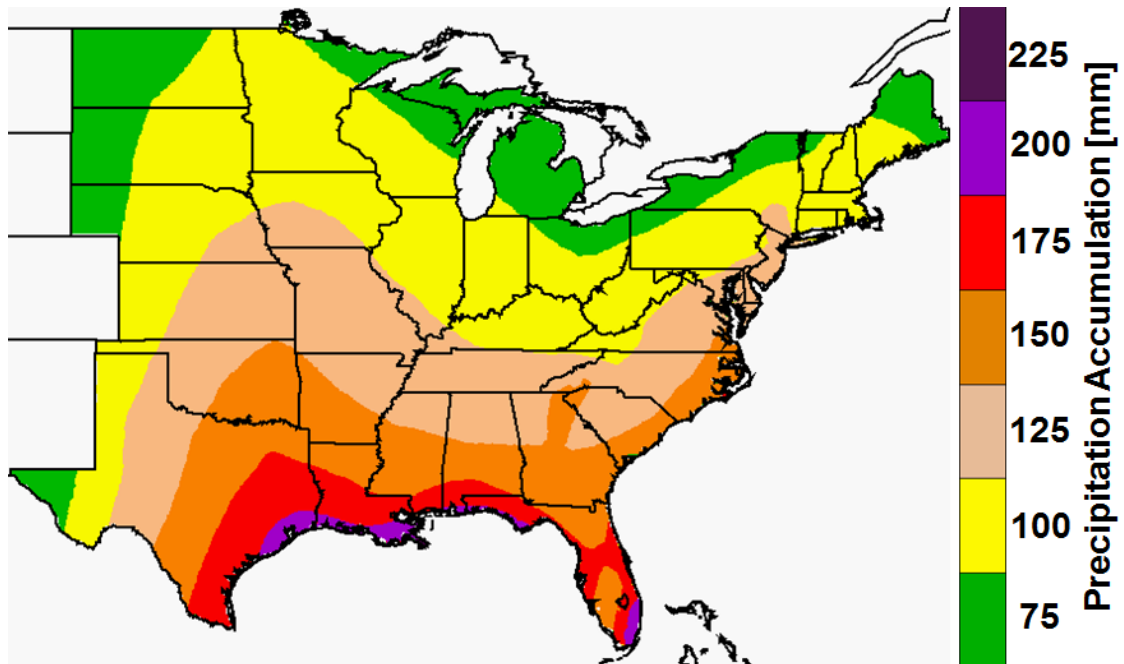


Figure 4.1: Hershfield 50-year, 6-hour recurrence interval for precipitation. (reproduced from Stevenson and Schumacher 2012)

Table 4.1: Heavy precipitation events by month and year. Only quality controlled cases included. Note the warm season focus implicit in the definition used.

Heavy Precipitation Cases			
	2010	2011	Totals
Jan	*	0	0
Feb	*	0	0
Mar	*	0	0
Apr	*	1	1
May	*	6	6
Jun	*	11	11
Jul	*	25	25
Aug	4	17	21
Sept	9	7	16
Oct	3	0	3
Nov	0	1	1
Dec	0	*	0
Totals	16	68	84

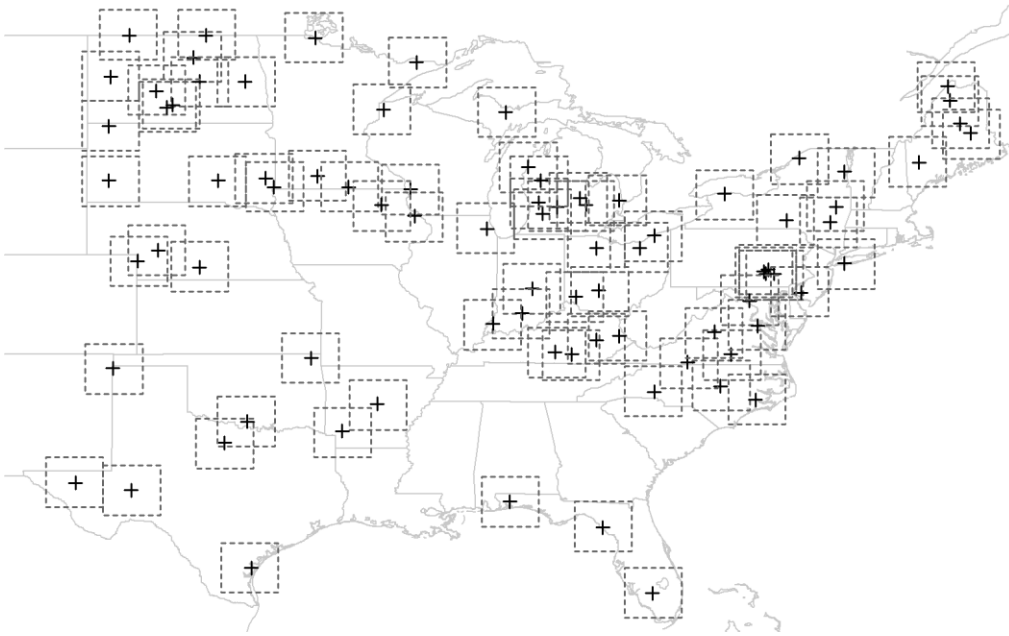


Figure 4.2: Heavy precipitation event center points and 200 km square domains for the 84 events between August 2010 and November 2011. Crosses indicate the center point of the domain, where the recurrence interval was crossed.

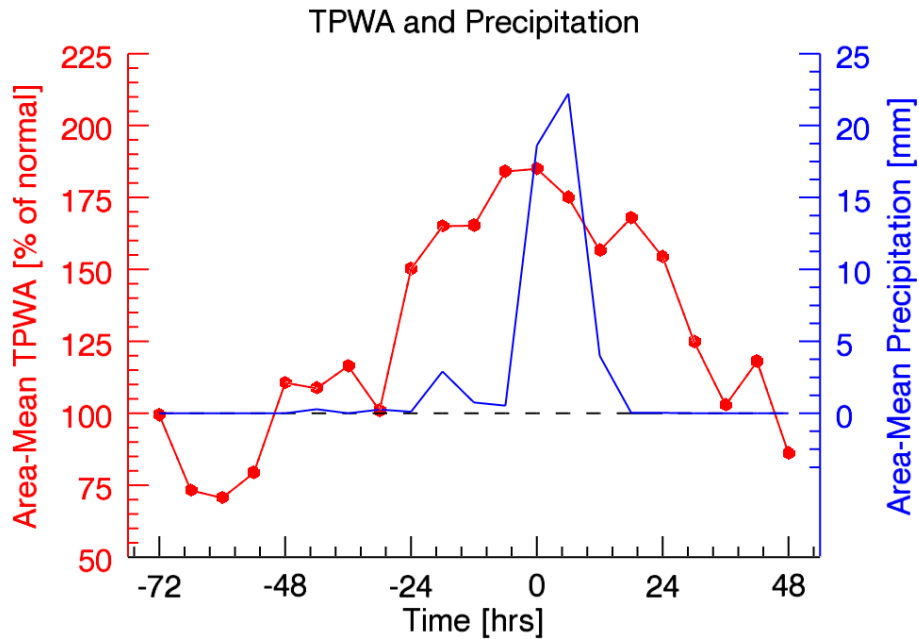


Figure 4.3: A classic heavy precipitation event, 0600 UTC 28 July 2011, from an area-mean TPWA (red) and precipitation (blue) perspective. The time series is labeled in reference to the event time, 0 hours, with a baseline (black dashed) for reference.

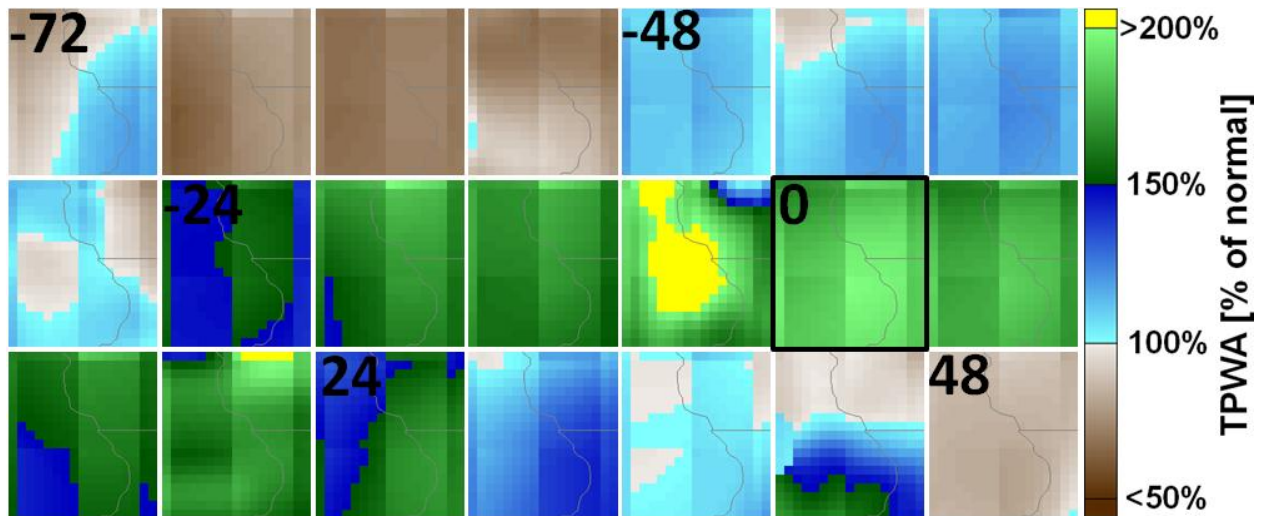


Figure 4.4: Sample TPWA spatial map series for the 0600 UTC 28 July 2011 heavy precipitation event. Time progresses from left to right, top to bottom, with the event time highlighted by a black box. The domain is centered in eastern Iowa, and is 200 x 200 km.

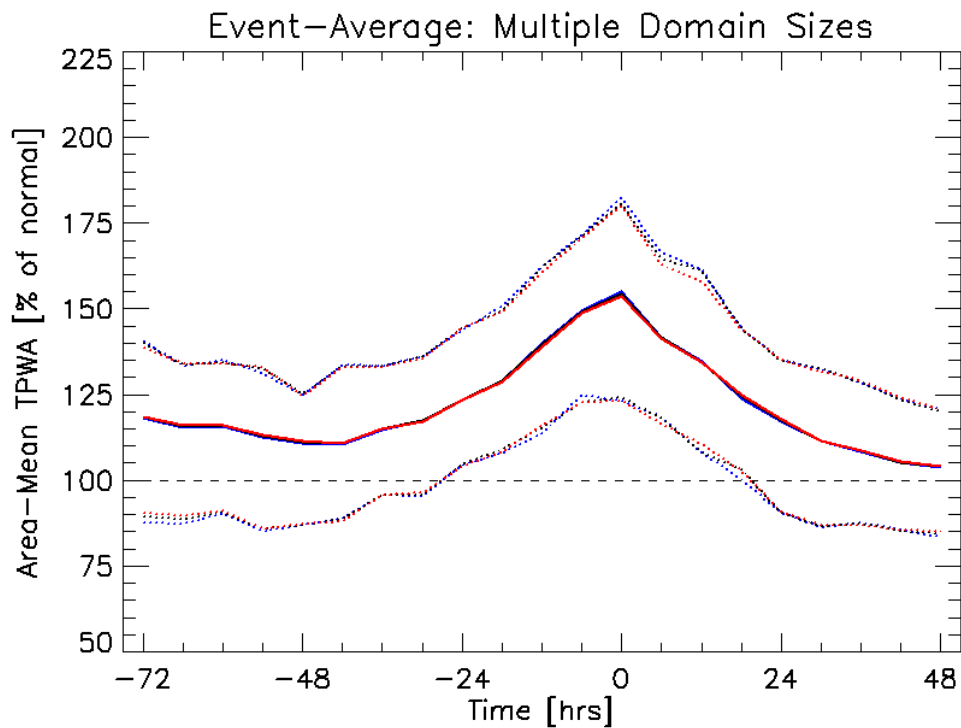


Figure 4.5: Event-average area-mean TPWA time series (solid) for various domain sizes: 160x160 km (blue), 200x200 km (black), and 250x250 km (red). Upper and lower quartiles (dotted) are shown as well.

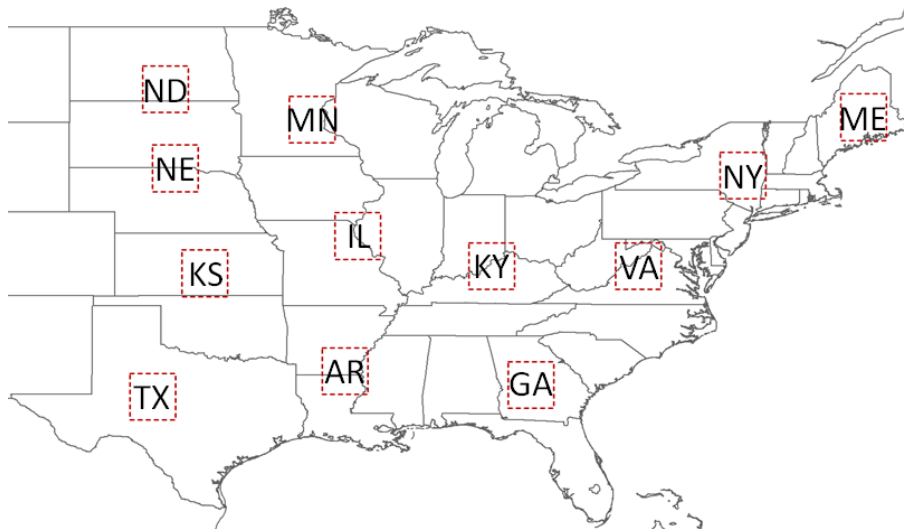


Figure 4.6: The locations and names of the 12 forecasting locations. The domains are 200 x 200 km: the same size used in heavy precipitation event analysis.

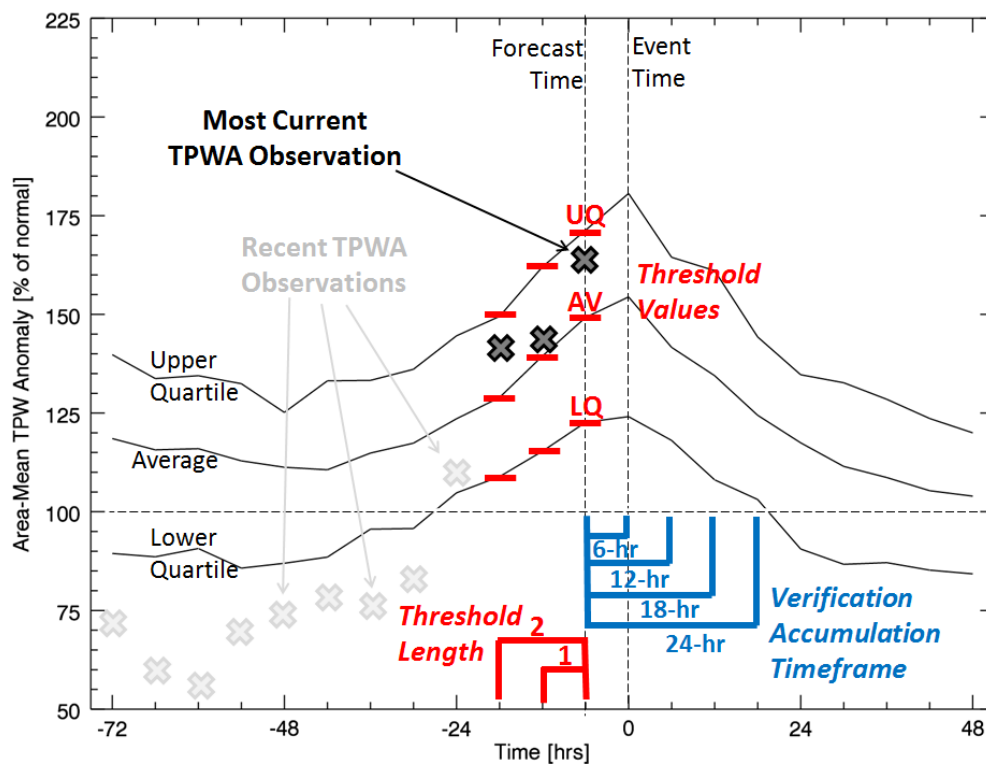


Figure 4.7: Diagram showing the different parameters that were adjusted when making threshold variations for the forecasting algorithm. Red labels show parameters that are changed in TPWA. Blue labels refer to parameters that are changed in precipitation. Black and grey values are the current and recent TPWA observations. The current time is always assumed to be -6 hours, i.e. a precipitation event could occur at any time.

		Observed?		
		Yes	No	
Forecast?	Yes	hit	false alarm	total forecast yes
	No	miss	correct negative	total forecast no
		total observed yes	total observed no	

Figure 4.8: Dichotomous contingency table. For this work, a “forecast” is defined as crossing the currently set TPWA threshold, and an “observed event” is exceeding the currently set precipitation threshold. The blue circle shows the categories needed for POD, whereas the red shows those needed for FAR. The grey circles are total values included for reference on POD & FAR barplots in section 5.

5. RESULTS

5.1 Composite Heavy Precipitation Events

The 84 event-average area-mean TPWA time series for the 200 x 200 km domain is shown in Figure 5.1. The most striking feature is the distinct bulge in TPWA centered at the event time. Mean TPWA rises before the event time, is maximum at event time, and decreases afterward. Individual events follow a much looser pattern, but only very rarely (in 3 events) is TPWA below normal at the event time. Mean TPWA peaks at 154% with the upper and lower quartiles at 181% and 124% respectively. The upper and lower quartiles are generally evenly spaced about the mean by about 25% on either side, implying an even distribution around the mean for most timesteps. However, the beginning 5 timesteps (from -72 to -48 hours) show the upper quartile closer to the mean than the lower quartile. This is evidence of very high individual values from a small number of events which are serving to raise the mean. The individual cases responsible are seen as the dotted lines surpassing 225% of normal for the first few timesteps. Further investigation shows these to be events in late September/early October 2010 along the East Coast where a strong, slow-moving coastal low-pressure system brought abundant oceanic moisture into the event domains. This exceptional, late warm season event caused high TPWA values via both high moisture content in blended TPW (via strong, moist-air advection), and low values in the NVAP climatology (due to time of year).

The timesteps immediately preceding the event time in Figure 5.1 are most interesting to the forecaster. In order to predict similar events using solely TPWA, a threshold must be derived which accurately diagnoses features of TPWA evolution and alerts the forecaster of an upcoming potential heavy precipitation event. This is done by using the information gained from the statistical analysis of the 84 past events. The values for the (upper quartile, average, and lower

quartile) are noted for the -18, -12, and -6 hour timesteps: (149,129,109), (162,139, 115), and (171,149,123) percent of normal, respectively. These values are summarized in Table 5.1 were applied to develop the forecasting tool described in section 4.5.

Spatial TPWA information was retained during the heavy precipitation event analysis. The event-average TPWA spatial distribution is displayed in Figure 5.2 as composite maps. These maps compliment the area-mean TPWA time series (Fig. 5.1) and show a number of additional interesting features. From -72 to -42 hours, little of interest occurs. This corresponds to the time when TPWA is slightly elevated, yet nearly constant in time in the area-mean time series (Fig. 5.1). At -36 hours TPWA begins to increase in the event domain. The transition to higher TPWA is not uniform across the domain, as higher values lie in the southwestern quadrant. This suggests that moist air is preferentially advected into the domain from the southwest during these time periods, similar to the findings presented by Moore et al. (2003) and Schumacher and Johnson (2005). This pattern enhances until -6 hours when the southern half of the domain becomes more moist than the northern half. The eastern half of the domain contains the most water vapor at the event time, with TPWA values between 150 and 160% of normal. From 6 to 30 hours, the domain dries out from west to east. By 48 hours after the event, the entire domain is near the climatological normal indicated by 100% TPWA.

A basic knowledge regarding synoptic and mesoscale weather patterns in the U.S. allows one to confirm the reasonability of the composite map results. Heavy rainfall is often found along MCSs and synoptic-scale fronts. These features often have a warm sector in the southeastern quadrant with southerly to southwesterly flow advecting moist air toward their center (Moore et al. 2003; Martin 2006). In the -36 to -6 hour time period, broad-scale, warm/moist-air advection likely occurs for many events. This manifests itself as a moistening of

the southwest quadrant. As the rain-producing meteorological features approach, and the circulations associated with them have a greater influence on the domain, and winds shift to a more southerly direction bringing increasing moisture northward. Moisture fuels heavy precipitation, causing the highest TPWA values to occur at event time. As a system moves through and exits a domain, the atmosphere dries out. Cold/dry air advection is often from the west or northwest, and the signal in the 84 cases composited suggests a preference for westerly drying flow.

Precipitation is a less continuous variable than TPWA. This is seen in Figure 5.3, which shows area-mean precipitation plotted for the 84 heavy precipitation events. As expected by its definition, the event time has the largest amount of precipitation by a large margin. Individual events have peaks at other times, but these only affect the average modestly, indicating no systematic secondary peaks. Average precipitation accumulation quickly drops on either side of the primary peak, indicating that precipitation in the domain size chosen (200 x 200 km) most often occurs on timescales shorter than 6 hours. The mean precipitation does not fall between the upper and lower quartile for time periods between -72 to -24 hours, or between 12 to 48 hours. This is result of averaging which includes many zeros and a few large numbers. In fact, the lower quartile shows that over 25% of cases contain no precipitation outside of the 18 hours encompassing the event time. The event time quantitative precipitation values for the upper quartile, average, and lower quartile are 24.5, 18.2, and 10.2 mm respectively.

The 18.2 mm average found for these heavy precipitation events was initially used as the precipitation threshold required in verification. However, very few events cross this high threshold, therefore precipitation thresholds of 6 and 9 mm were examined. Lowering the

precipitation thresholds to these values leads to the forecasting tool being tested on how well it observes moderate precipitation as well as heavy precipitation, not simply heavy precipitation.

5.2 Forecast Tool Verification

Some locations perform better than others, implying that regional differences in warm-season TPWA evolution characteristics affect forecast performance. Furthermore, the strict definition of what is an “observed” event hinders the forecast skill, which is demonstrated by analysis of two pairs of TPWA and precipitation time series: hits, misses, and false alarms are labeled to show where the forecast tool is being verified for hits, and where it is being penalized for misses and false alarms. Plots were also created for a number of threshold variations to illustrate the probability of detection (POD) and false alarm ratio (FAR) for the 12 forecasting locations. On the far right of each graph, the 13th pair of bars shows the location-average POD and FAR, as well as the total forecasts and observed events, to give an overall sense for that particular threshold variation’s performance.

Figure 5.4 shows the results of requiring TPWA to be rising for at least 6 hours before crossing a TPWA threshold of 149%, which was chosen based on the average -6 hour value from heavy precipitation event analysis. Figure 5.4a sets an “observed” event as one which exceeds an area-mean precipitation accumulation of 6 mm; Figure 5.4b requires at least 9 mm for a precipitation event to count as an observed event. The number of forecasts made between (a) and (b) is identical, 598, because the TPWA threshold is constant between the two graphs. However, the number of observed events, 288 in (a) and 154 in (b), changes because the definition of an observed event becomes more restrictive in (b), increasing from at least 6 mm to at least 9 mm. The POD is 29% on average when using 6 mm, but increases to 37% for 9 mm. This indicates that as a precipitation event becomes greater in magnitude, there is a better chance that the

algorithm will correctly predict its occurrence. The POD is low in both cases, showing poor performance: Only one out of every three or four events will be detected by this algorithm variation. The FAR is 85% for the 6 mm and 90% for the 9 mm. The increase in this statistic as one goes from 6 mm events to 9 mm events is due to fewer observations of 9 mm events, as well as an increased tendency for TPWA to rise sufficiently to trigger a forecast without receiving at least 9 mm of precipitation 6 hours later. These FAR values also show poor performance: 17 or 18 out of every 20 forecasts never verify.

Certain individual locations demonstrate more forecast skill than the average. Figure 5.4a shows that the Kentucky location produces the lowest percentage of false alarms, namely, 76%. This number is closer to a number that can be used operationally. POD for the Maine location is 54%, indicating that over half of the observed events were forecast correctly. After raising the precipitation threshold to 9 mm (Fig. 5.4b), POD reaches nearly 60% for 4 of the locations: KS, MN, GA, and VA. For these locations, TPWA evolution more closely follows the average evolution based on heavy precipitation events, leading to the algorithm's increase in skill. This indicates that tailoring the tool to particular locations in future work may serve to increase its usefulness.

Figure 5.5 shows the same statistics as Figure 5.4, but the TPWA threshold value is lowered from 149% to 123% of normal, which is based on the lower quartile heavy precipitation event analysis. One effect of this change is an increase in the number of heavy precipitation events forecast: from 598 in Figure 5.4 to 1471 in Figure 5.5. Notice that the number of observed events is constant between the two figures, because the precipitation thresholds used do not change. The lowering of the TPWA threshold causes the POD to rise dramatically. This change is logical, since as one lowers the TPWA threshold, the chance that the threshold will be reached

increases, thus triggering more forecasts. POD reaches 52% on average for the 6 mm precipitation threshold (Fig. 5.5a), and is over as 65% for 3 locations: KS, NY, and ME. For the 9 mm threshold (Fig. 5.5b), POD is even higher, at 57% on average, and breaks 70% at 4 locations. These values approach what would be desired for an operational forecasting aid, but this is not the entire story. The increase in POD gained by lowering the TPWA threshold is not accomplished without negatively affecting FAR. FAR for most location exceeds 85% for the 6 mm threshold (Fig. 5.5a), and surpasses 90% for the 9 mm precipitation threshold (Fig 5.5b). These values show that many false alarms occur when expecting precipitation 6 hours following the TPWA threshold being reached, and show that the thresholds specified in Figure 5.5 are of limited use for forecasters who desire to minimize FAR.

Figures 5.6 and 5.7 display the same statistics as Figures 5.4 and 5.5, save for the requirement that TPWA must be rising for at least 12 hours preceding threshold exceedance. Notice that the number of forecasts made now decreases significantly for both the average-based, and lower quartile-based TPWA thresholds. This is due to the 12-hour threshold length parameter being a stricter requirement than the previously set 6-hour parameter. The number of events observed remains nearly constant between the two sets of figures, with the only differences arising due to missing TPWA data (TPWA must be available for the entire time range being analyzed for stats to be computed).

Figure 5.6a shows that the number of forecasts made is close to the number of events observed, 362 to 286, respectively. However, there is only a 16% POD on average. This value is increased to 21% by using a larger precipitation threshold, which is shown in Figure 5.6b, but the value is still low compared to operational forecasting goals. The Minnesota forecasting location shows the most promising results with a POD of nearly 40% for 6 mm, and 55% for 9 mm. False

alarms remain an issue, occurring nearly 85% of the time on average for the 6 mm precipitation threshold (Fig. 5.6b), and 90% of the time for the 9 mm threshold (Fig. 5.6b).

Figure 5.7 uses a 12-hour rising, lower quartile-based TPWA threshold. The effect is similar to that described for Figure 5.5, in that POD rises at the cost of rising FAR. In the most extreme cases, the algorithm misses all of the few events which occur, and POD is 0% and FAR is 100%. These results call attention to the need for a longer time period for verification before this tool can be used operationally.

Overall, the forecasting tool performance as tested in this work is below expectations of operational forecasters. An additional close analysis at individual locations reveals a few key issues regarding the tool's poor performance, and offers hope that future work may serve to increase the aid's usefulness.

Figure 5.8 and 5.9 shows the 6-month time series of area-mean TPWA and precipitation used when calculating POD and FAR. Labeled on the time series are the hits, false alarms, and misses produced by the algorithm. Correct negatives are not labeled explicitly, as they were not used in any of the verification scores analyzed for this research. The algorithm variation shown is the 12-hour length, average value based TPWA threshold with a 6 mm precipitation threshold.

On April 10th, in Minnesota, (Fig. 5.8) one can see that the algorithm is being punished in verification scores for alerting the forecaster of an imminent precipitation event over 6 hours in advance. In other words, the algorithm often gives more than 6 hours of lead time. This is shown by false alarms (vertical lines) which occur immediately prior to a hit (diamond) or miss (dot). This occurs again during the end of April, in mid-May, in early July, and in mid-July. Figure 5.9 demonstrates a similar phenomenon is occurring at the New York location during mid-April, early May, early June, late July, and late September. Although close analysis of these figures

shows that the forecasting tool is far from perfect, they also demonstrate that restricting the definition of an “observed event” to a precipitation threshold crossed exactly 6 hours later has a detrimental effect on the verification scores for the forecasting tool. Modifying the definition of what is an observed event may help increase algorithm forecast skill if lead times are better quantified. It is also possible that TPW evolves in a manner sufficiently complex to cause any algorithm, based on the methodology presented here, to produce timing errors.

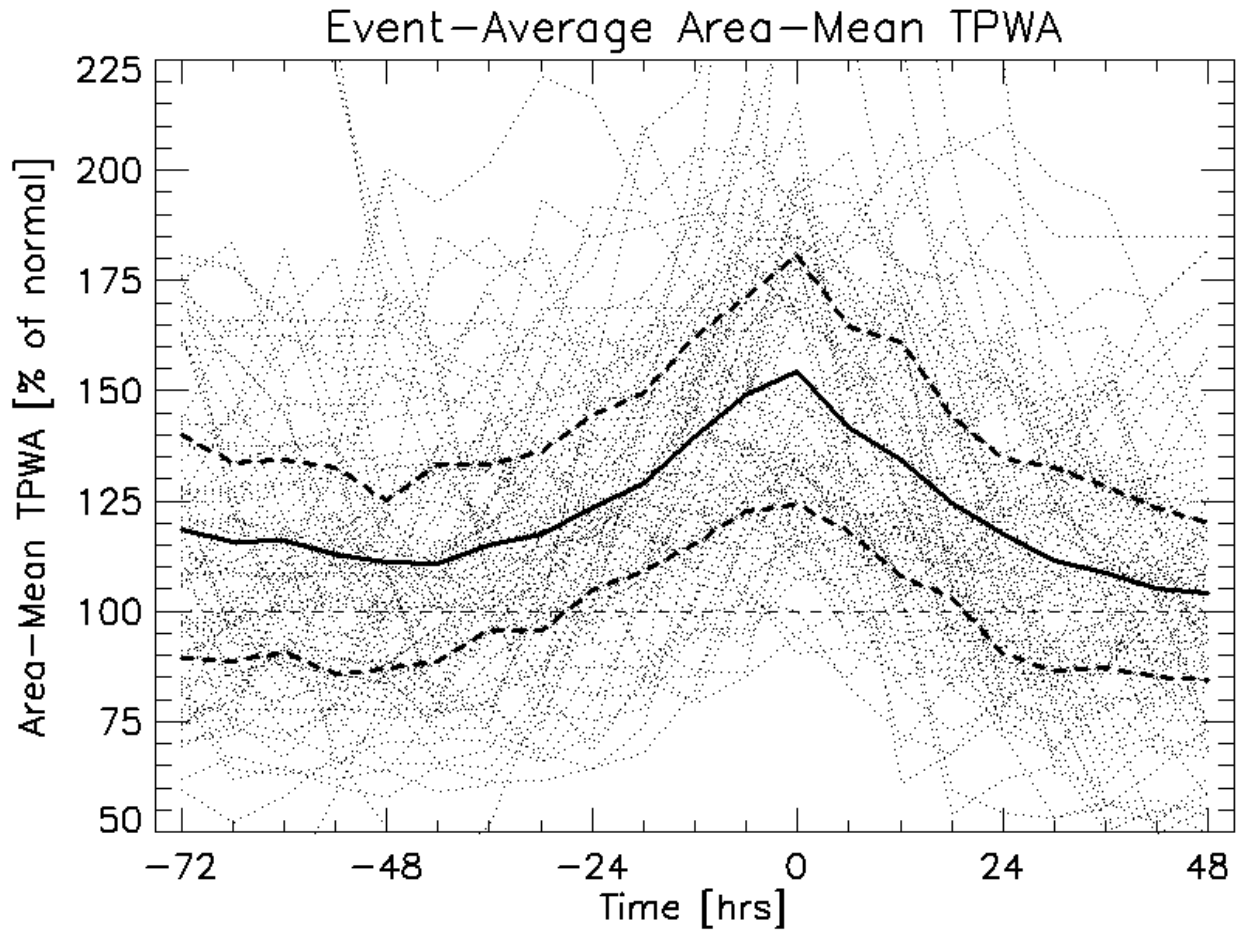


Figure 5.1: Event-average area-mean TPWA time series (thick solid), upper and lower quartiles (thick dashed), normal line (thin dashed), and individual event area-mean TPWA (thin dotted).

Table 5.1: The statistically derived TPWA values for the forecast hours leading up to the event time. These values are used in the forecasting algorithm when setting the “threshold values” parameter.

		Forecast Hour			
		-18	-12	-6	0
Average TPWA	Upper Quartile	149	162	171	181
	Average	129	139	149	154
	Lower Quartile	109	115	123	124

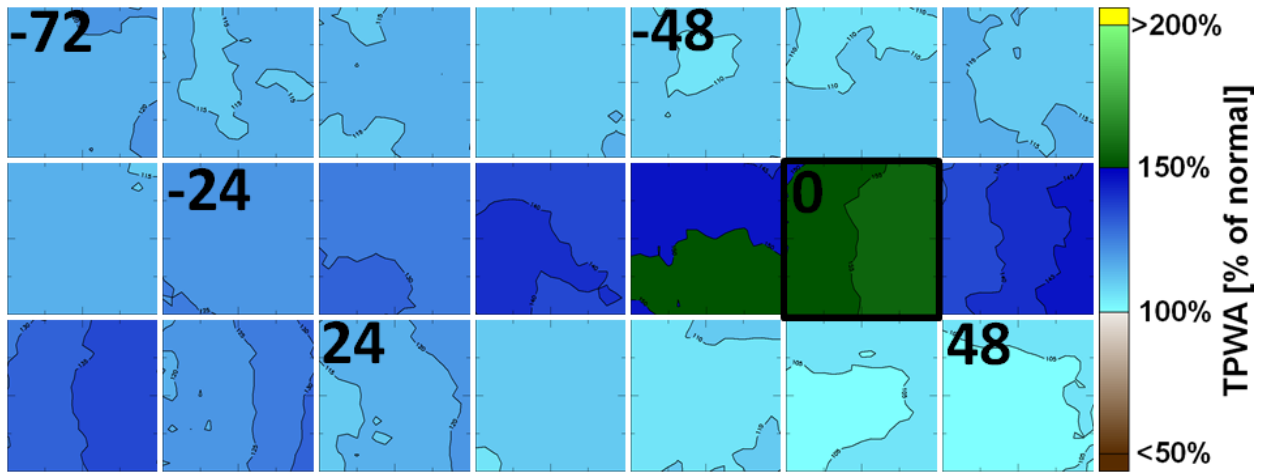


Figure 5.2: Event-average TPWA spatial map series, contours every 5%. Time progresses from left to right, top to bottom (bold black numbers), with the event time highlighted by a black box.

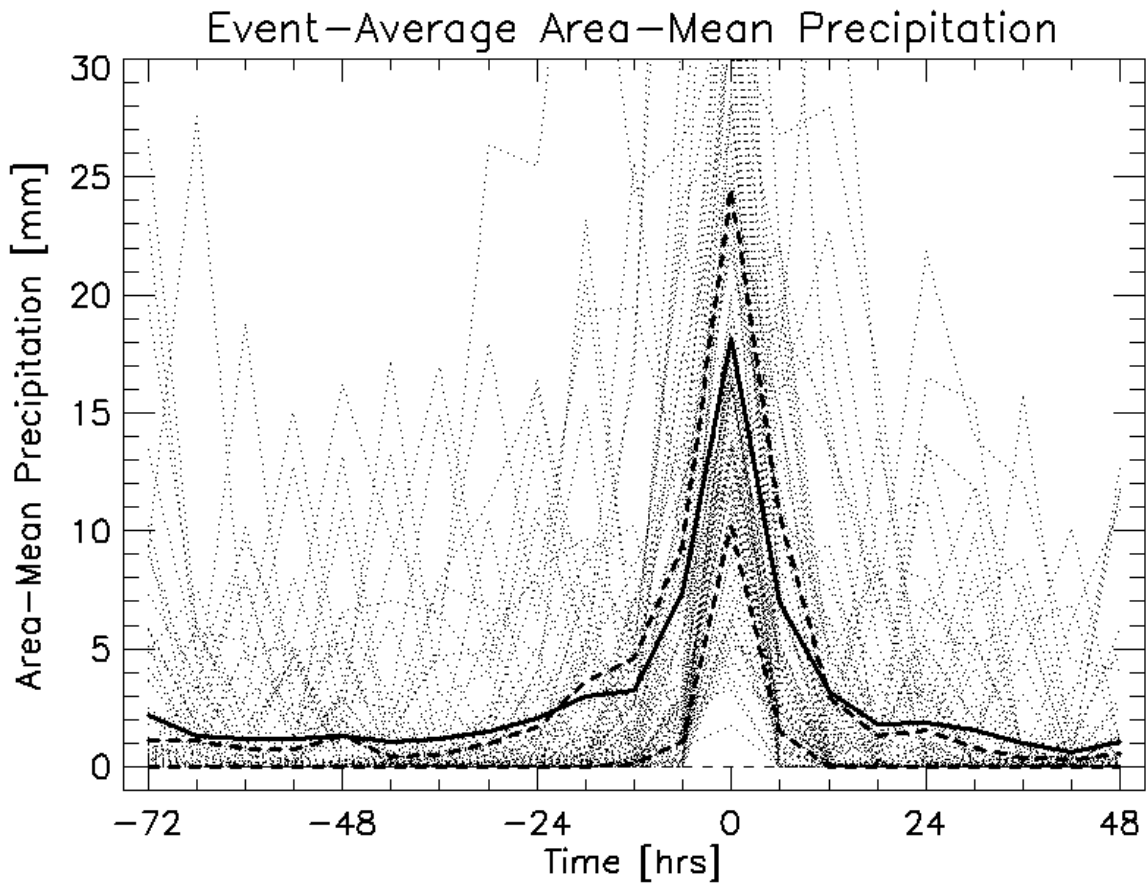


Figure 5.3: Event-average precipitation time series (thick solid), upper and lower quartiles (thick dashed), normal line (thin dashed), and individual event area-mean precipitation (thin dotted).

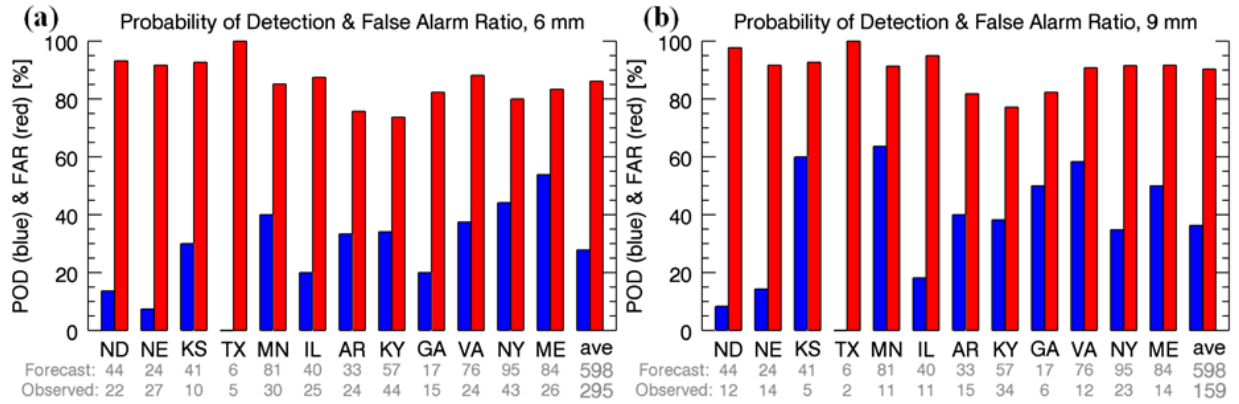


Figure 5.4: The POD (blue), FAR (red), total forecasts, and total observed events for the 6-hour length, average value TPWA threshold. Individual locations and the all-location average are shown for the (a) 6 mm and (b) 9 mm precipitation threshold.

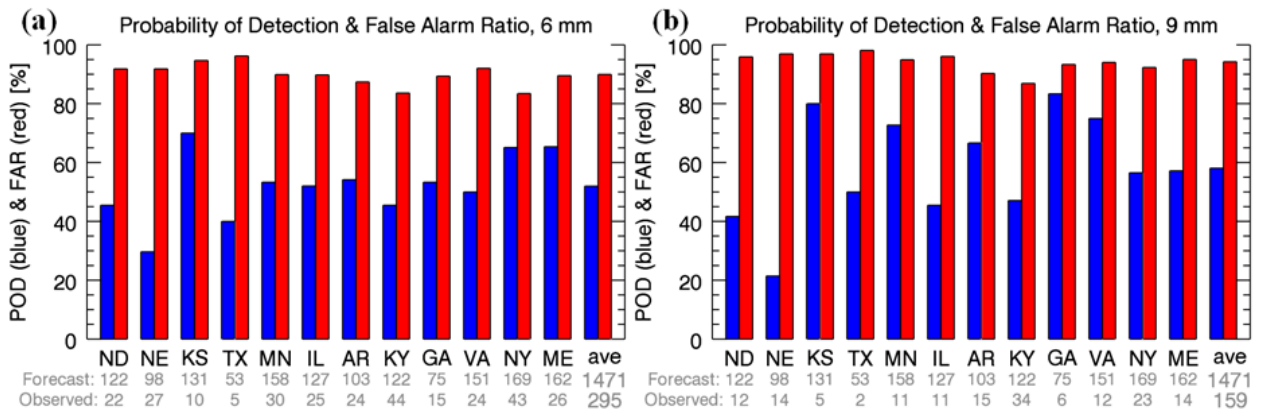


Figure 5.5: The POD (blue), FAR (red), total forecasts, and total observed events for the 6-hour length, lower quartile value TPWA threshold. Individual locations and the all-location average are shown for the (a) 6 mm and (b) 9 mm precipitation threshold.

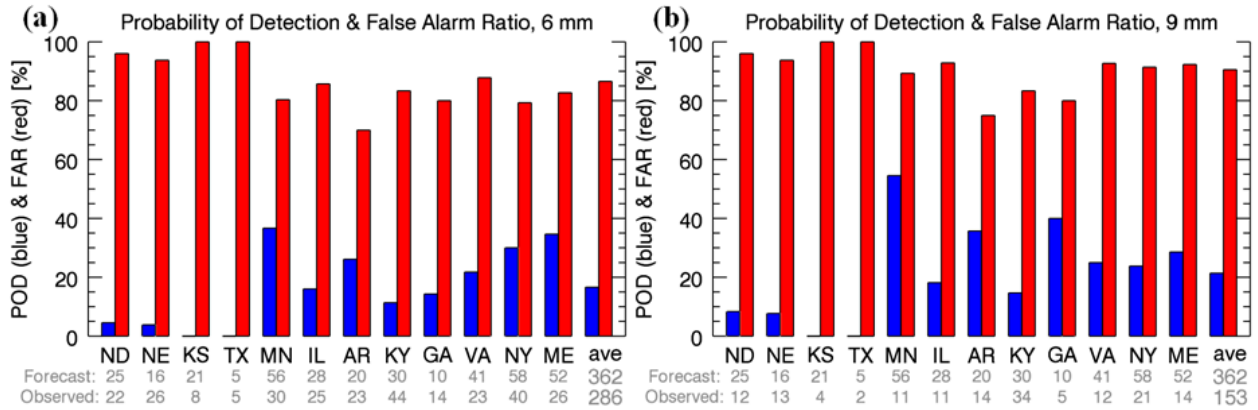


Figure 5.6: The POD (blue), FAR (red), total forecasts, and total observed events for the 12-hour length, average value TPWA threshold. Individual locations and the all-location average are shown for the (a) 6 mm and (b) 9 mm precipitation threshold.

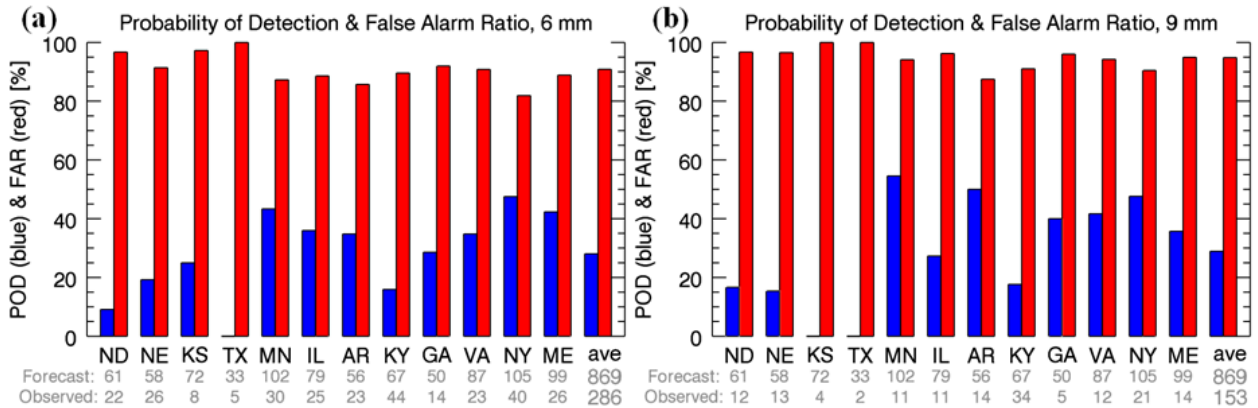


Figure 5.7: The POD (blue), FAR (red), total forecasts, and total observed events for the 12-hour length, lower quartile value TPWA threshold. Individual locations and the all-location average are shown for the (a) 6 mm and (b) 9 mm precipitation threshold.

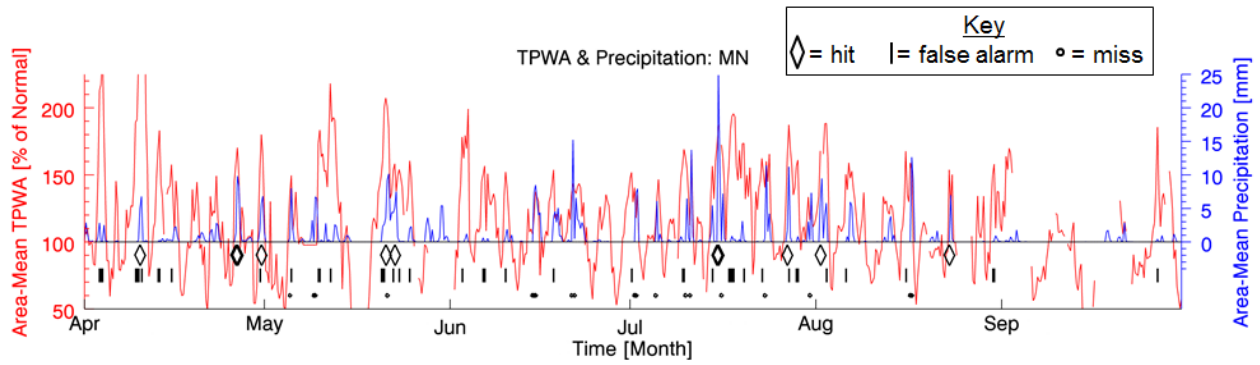


Figure 5.8: Area-mean TPWA and Precipitation for the Minnesota forecast location from April through September 2011. Hits, false alarms, and misses are labeled for the 12-hour length, average value TPWA threshold with the 6 mm precipitation threshold.

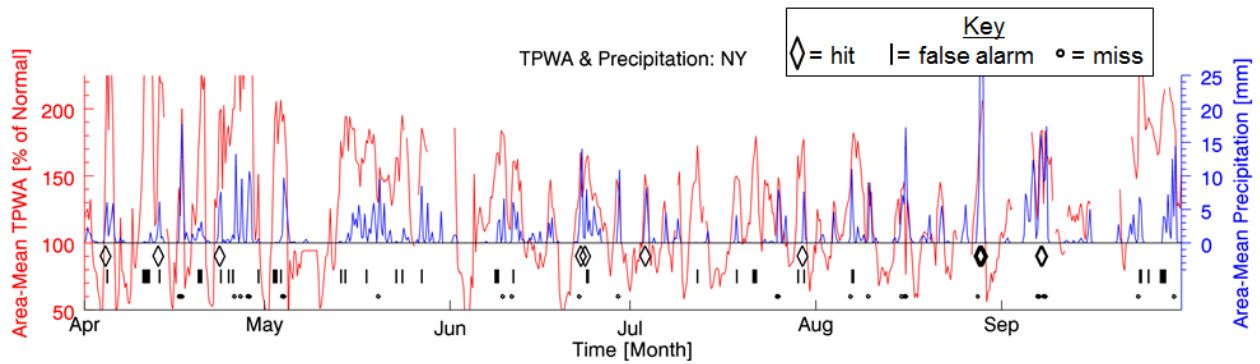


Figure 5.9: Area-mean TPWA and Precipitation for the New York forecast location from April through September 2011. Hits, false alarms, and misses are labeled for the 12-hour length, average value TPWA threshold with the 6 mm precipitation threshold

6. SUMMARY AND CONCLUSIONS

6.1 Research Conclusions

The hypothesis that TPWA will be positive and increasing preceding heavy precipitation events in the central to eastern U.S. is supported. On average, TPWA rises continually in the 36 hours preceding a heavy rain event, reaching 149% of normal 6 hours before the precipitation event and peaking at 154% of normal at the event time. Spatial maps suggest moist transport into the mesoscale domains from the southwest and south preceding the event. TPWA values decrease from west to east in the domain as dry westerly flows likely becomes dominant after an event. These results align well with the understanding of flow patterns associated with synoptic mid-latitude cyclones and mesoscale convective systems, bringing credibility to the methodology used to study the events (Moore et al. 2003; Schumacher and Johnson 2005). The signal of increasing, positive TPWA anomalies in the domains surrounding these heavy precipitation events strongly encouraged the development of a precipitation forecasting tool which utilizes the TPWA trend.

The forecasting tool's performance is lackluster for most locations when using the methodology described. It shows low probability of detection and high false alarm rates for moderate precipitation events. Heavy precipitation occurs rarely over the time period selected which hinders verification efforts for heavy precipitation alone. The poor performance of the simple forecast tool suggests that precipitation formation requires more than moist ambient air, supporting previous studies (Maddox et al. 1979; Doswell et al. 1996; Junker et al. 1999). Other ingredients, such as a source of lift via quasi-geostrophic dynamics, convergence, orography, or convection, play a major role (Doswell et al. 1996; Martin 2006). Nevertheless, the TPWA forecast tool could still serve in its current state as an operational forecast aid for mesoscale

regions by heightening forecaster awareness, or simply as a research tool. A moistening domain indicated by increasing, positive TPWA values implies increased probability of precipitation, as one of the necessary ingredients, moisture, is shown to be present. Finally, skill of the forecast tool is not independent of location or time of year. Regions where TPWA evolution more closely follows the model of the threshold chosen tend to perform better when using dichotomous contingency table verification scores. Seasonality has an effect as well, with larger anomalies occurring in the spring and autumn. A few locations approach NWS tornado warning goals for probability of detection and false alarm rate. This is encouraging and impressive seeing as how only one variable, atmospheric moisture, is examined by the methodology presented here.

Rare events are difficult to predict. Heavy precipitation, as defined in this work, occurs on average every 50 years for a location. Tools that predict rare events often suffer from a large number of false alarms, but this can be overcome using multiple data sources. The low performance of the forecasting tool developed in this work encourages forecasters to use whatever supplementary data are available when trying to predict rare events. TPWA is one of many valuable variables when attempting to predict heavy precipitation, but certainly does not tell the whole story.

6.2 Research Limitations

The TPWA dataset used in this research is not a complete, operationally archived dataset at this time. NOAA NESDIS does operationally produce the product for hourly display, but the National Climatic Data Center (NCDC) does not yet archive data. This is unfortunate, since data voids would be minimal if NCDC maintained an archive, and hourly data would be easily available. CIRA at Colorado State University, the original developers, have an extensive archive of 6-hourly data available which were used for this research. However, it is not an “operationally

archived” dataset, meaning there are times when data are lost or not computed due to power outages, computing power limitations, etc. Therefore TPWA was the dataset that often hindered heavy precipitation events from being used. Also, missing data periods for TPWA lowered the strength of statistics used to verify the forecasting tool, as times where TPWA was not available had to be ignored, even though information for precipitation was present.

The methodology described is only tested in the United States, which is a notably data-rich region of the globe. This region was chosen to ensure that the forecasting tool could be verified; however, one objective of using such a simple methodology was to provide evidence for the usefulness of a satellite-data-based forecasting tool for data-denied regions. Since the tool was not verified over data-denied areas, it has yet to be shown whether the results of this work are generalizable to the entire globe. Qualitative analysis of hundreds of global TPWA maps indicates that the forecasting tool would likely perform similarly to the results shown here in most mid-latitude regions. The tropics have a very different dynamics, as well as a low range of TPWA values, indicating that a different methodology would need to be applied there. The high-latitudes introduce the problem of missing data over ice and sea ice, as well as an extreme range of TPWA. The high latitudes would therefore also likely require a different methodology to examine the usefulness of TPWA for precipitation forecasting.

Quantitative lead times were not tested. Not only is this a common metric for verification of forecast skill, but it also influences the results of verification shown in this research. Lead time is assumed to be 6 hours via the verification methodology, but lead times are often greater than this, as shown in the verification time series. This potential benefit of using TPWA is ignored, and the forecast aid is penalized leading to decreased forecasting skill as measured by the methodology used here.

Finally, spatial averaging reduces the usefulness for true “point forecasting”. Using mesoscale-sized domains is reasonable for many applications: military battlespace situational awareness, NWS zone forecasting, etc. Nevertheless, if a user needs to know whether a particular point location will receive rainfall, the methodology is not tailored to this user’s needs. Figure 6.1 shows a variety of precipitation accumulation distributions and their equivalent area-mean value. These examples demonstrate the wide variety of accumulations which can lead to high values in an area-mean. Users must be aware of this limitation.

6.3 Future Work

The large number of future directions for TPWA research using methodologies similar to those used in this work is encouraging to the authors. The methodology used to test heavy precipitation events proved to be useful in understanding atmospheric moisture evolution from a TPWA perspective. The TPWA used was an observational dataset based on satellite products. One direction for future research would be to test a similar methodology with model-derived TPWA values. This would allow the researcher to study how well the weather prediction model is handling the moisture variable. The climatology dataset used could also be modified in order to test the effect of using observational vs. reanalysis climatology to determine TPWA. Some possible model-based TPW climatologies which could be used in future studies are the NCEP-NCAR Reanalysis-2 TPW described by Kanamitsu et al. (2002) or the Modern-Era Retrospective Analysis for Research and Applications (MERRA) TPW detailed by Rienecker et al. (2011).

Higher temporal resolution data could be used to investigate the impacts on forecast skill if NCDC begins to archive the hourly TPWA data they produce. Getting the most recent satellite

retrievals of TPW, along with hourly Stage IV precipitation (which is currently available), might allow events to be captured closer to the time at which they occur.

A limitation of the forecast verification is that it ignored incorporating lead times into verification. It may be worthwhile to develop a methodology to test and quantify lead time more accurately in order to better choose what will be considered an “observed” precipitation event in the verification testing. Using data-derived lead times to relax the requirement of precipitation following a crossed TPWA threshold by 6 hours may serve to increase “hits”, and therefore raise POD and lower FAR. Furthermore, TPWA could be examined per forecasting location to better develop unique TPWA thresholds based on a location’s climatology. The objective of getting a larger scale sense for TPWA evolution prevented the use of such a method in this work, but any operational forecaster desiring to use this tool for a particular location would be best served if the forecaster could quantify a location’s TPWA evolution prior to setting the TPWA threshold parameter in the forecasting tool. One method would be to reference a probability distribution curve (e.g. Fig. 6.2, 6.3, and Appendix I) for TPWA, and then set the TPWA threshold where XX% of the TPWA values are lower than that percent. The current study suggests higher percentage TPWA thresholds could be useful for the northern mid-latitudes, and lower thresholds may be useful for the southern mid-latitudes. Results shown in this work imply that such improvements could increase TPWA POD and reduce FAR. Furthermore, one could seasonally adjust the TPWA threshold to better account for spring, fall, or winter events. After completing these improvements, it would be interesting to compare the results of the simple forecast tool with current global weather prediction models. The simple tool would likely process faster for users who need a quick forecast aid, but it is hard to speculate on performance in comparison to the Global Forecast System (GFS), for example.

This work focused on area-mean precipitation. Instead, one could focus on the maximum precipitation point within a domain to characterize precipitation. Using such a method, the forecasting aid may better detect heavy precipitation events. Also, the tool would be focusing more on true “heavy precipitation” events, rather than on moderate to heavy events.

Incorporating more data to both heavy precipitation event analysis and forecasting verification would strengthen the statistics used in both sections. The CIRA TPWA archive goes back through 2006, and Stage IV precipitation data are available from 2006 to present as well. It may be interesting to subdivide the heavy precipitation events into categories based on type of meteorological system, annual average surface dew point, or latitude. Before this could be done, one would have to increase the number of heavy precipitation events analyzed to increase the number of events in each category. A few caveats would have to be considered before undertaking such a task. There are missing months, sometimes multiple in a row, for TPWA. Also, global, over-land TPW retrievals were not available before August 2010 since MIRS retrievals were not developed until that time.

TPWA data show anomalies on both ends of the spectrum: moist and dry. This work focused on the moist side of the spectrum. One could perform a “drought events” analysis in a similar fashion to what was done for heavy precipitation events. The domain and temporal considerations would have to be modified, but this is easily accomplished through a few parameter changes in the forecasting tool’s program.

Finally, it may be interesting to examine how event domain size affects TPWA evolution for heavy precipitation events statistics. The three mesoscale domains chosen and initially tested (160, 200, and 250 km square) in the heavy precipitation events analysis showed similar TPWA evolution. Under close inspection, even these similarly-sized mesoscale domains showed a trend:

as domain size increases, TPWA becomes less positive around a heavy precipitation event. In other words, the area-mean anomalies begin to “wash out” as you approach larger spatial scales. It would be interesting to vary domain sizes significantly to see the limits of an increasing signal showing up in TPWA. One might expect the synoptic scale (~1000 km box) to have a nearly normal area-mean TPWA, regardless of heavy precipitation event occurrence.

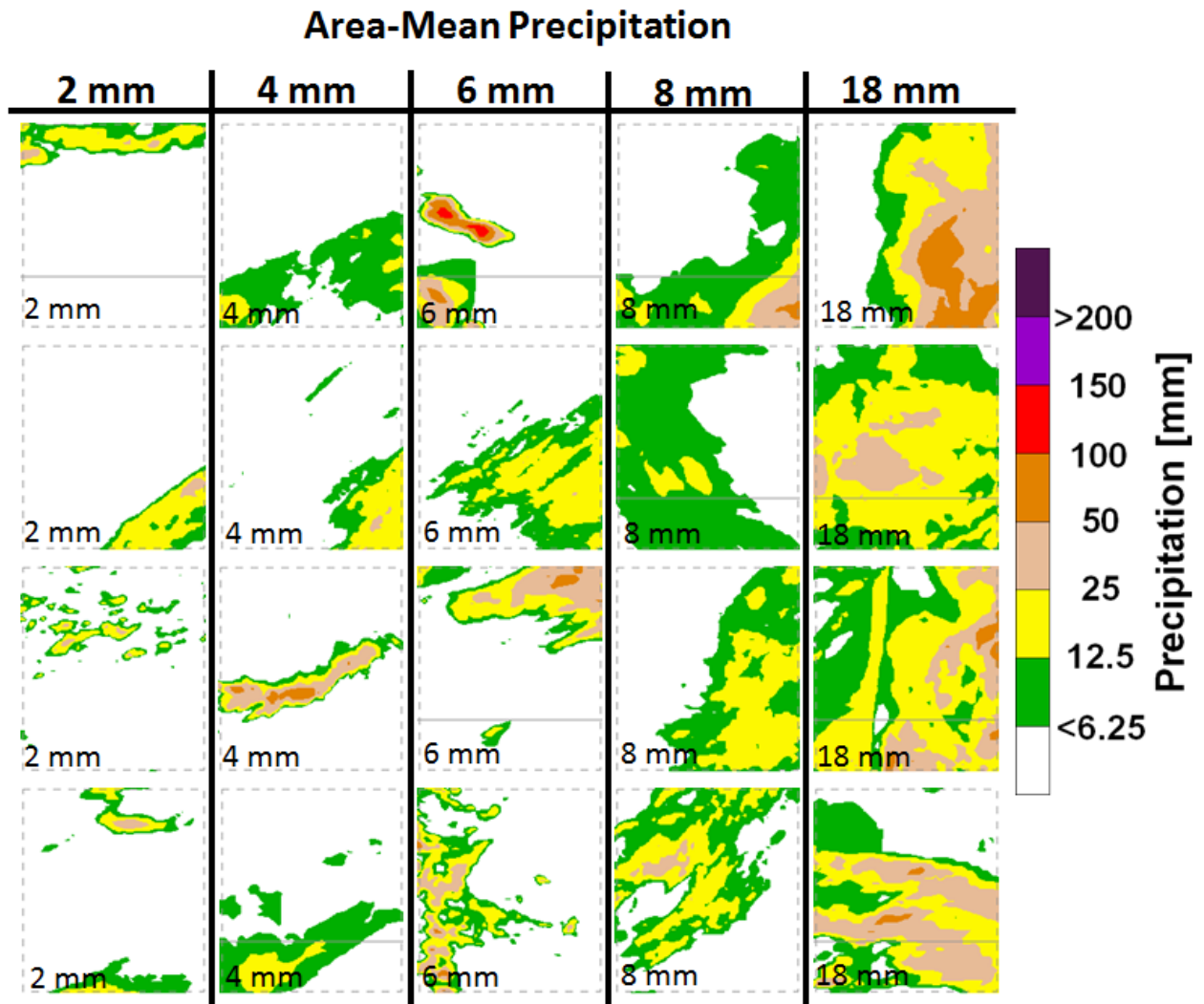


Figure 6.1: Example spatial distributions of 6 hour precipitation accumulations for 5 values of area-mean precipitation. Categories chosen based on forecasting results (2, 4, 6, and 8 mm) and statistical event analysis (18 mm). Precipitation is filled in color as shown, and has units of mm.

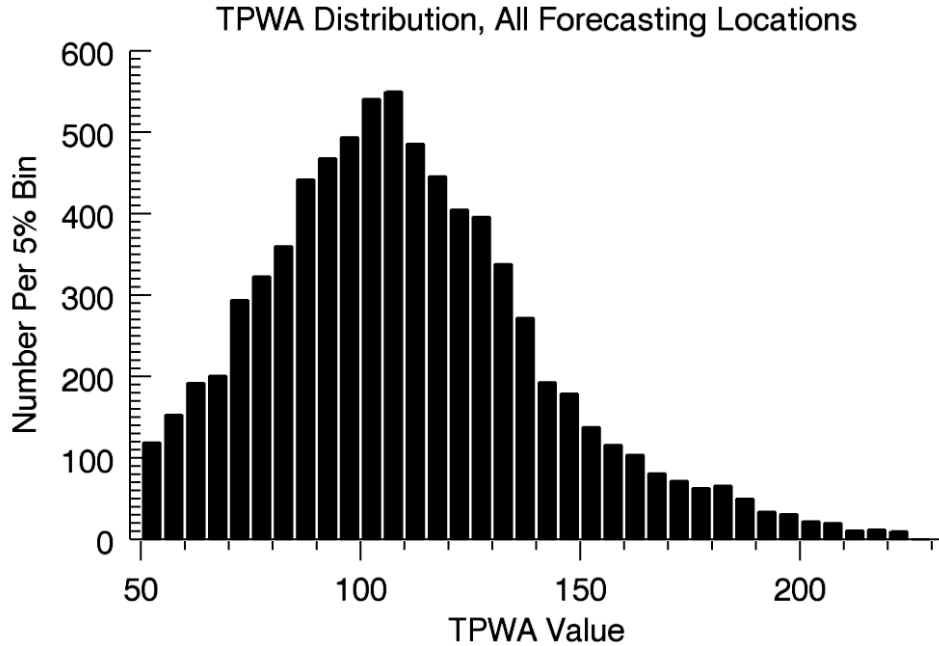


Figure 6.2: TPWA distribution using 5%-width bins for April through September 2011 for all forecasting locations.

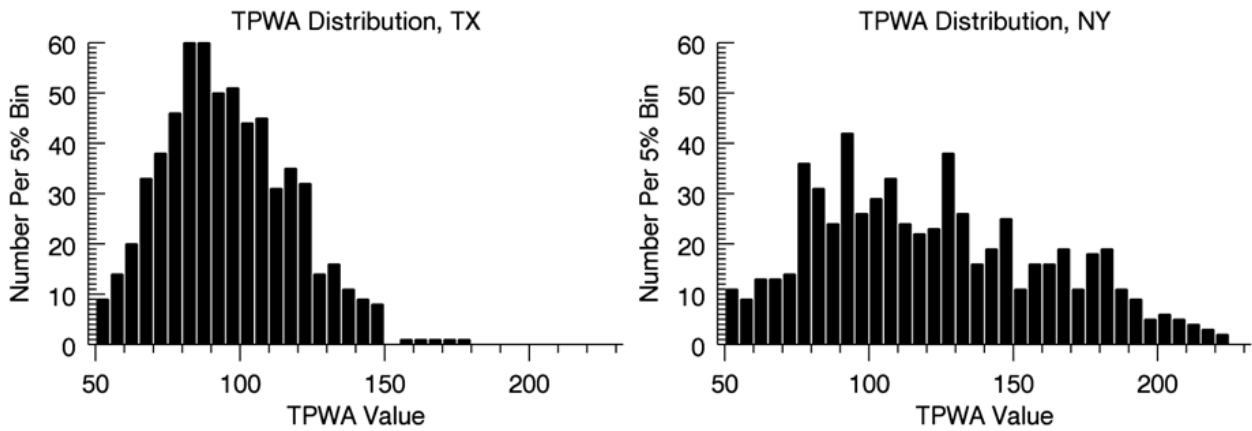


Figure 6.3: TPWA distribution using 5%-width bins for the months of April through September 2011 for the Texas and New York forecasting locations. Note the large differences between these two locations.

REFERENCES

- Ahnert, P., M. Hudlow, E. Johnson, D. Greene, and M. Rosa Dias, 1983: Proposed “on-site” precipitation processing system for NEXRAD. Preprints, *21st Conf. on Radar Meteorology*, Edmonton, AB, Canada, Amer. Meteor. Soc., 378–385.
- Amenu, G. G., and P. Kumar, 2005: NVAP and reanalysis-2 global precipitable water products. *Bull. Amer. Meteor. Soc.*, **86**, 245–256.
- AMS Glossary, cited 2012: Precipitable water. [Available online at <http://amsglossary.allenpress.com/glossary/>.]
- Ashley, S. T., and W. S. Ashley, 2008: Flood fatalities in the United States. *J. Appl. Meteor. Climatol.*, **47**, 805–818.
- Baldwin, M. E., and K. E. Mitchell, 1997: The NCEP hourly multisensor U. S. precipitation analysis for operations and GCIP research. Preprints, *13th Conf. on Hydrology*, Long Beach, CA, Amer. Meteor. Soc., 54–55.
- Bao, J.-W., S. A. Michelson, P. J. Neiman, F. M. Ralph, and J. M. Wilczak, 2006: Interpretation of enhanced integrated water vapor bands associated with extratropical cyclones: Their formation and connection to tropical moisture. *Mon. Wea. Rev.*, **134**, 1063–1080.
- Barnes, S. L., 1964: A technique for maximizing details in numerical weather map analysis. *J. Appl. Meteor.*, **3**, 396–409.
- Bevis, M., S. Businger, T. A. Herring, C. Rocken, R. A. Anthes, and R. H. Ware, 1992: GPS meteorology: Remote sensing of atmospheric water vapor using the global positioning system, *J. Geophys. Res.*, **97**, 15787–15801.
- Boukabara, S.-A, K. Garrett, and W. Chen, 2010: Global coverage of total precipitable water using a microwave variational algorithm. *IEEE Trans. Geosci. Remote Sens.*, **48**, 3608–3621.
- Browning, K. A., and C. W. Pardoe, 1973: Structure of low-level jet streams ahead of mid-latitude cold fronts. *Quart. J. Roy. Meteor. Soc.*, **99**, 619–638.
- Doswell, C. A., H. E. Brooks, and R. A. Maddox, 1996: Flash flood forecasting: An ingredients-based methodology. *Wea. Forecasting*, **11**, 560–581.
- Duan, J., M. Bevis, P. Fang, Y. Bock, S. Chiswell, S. Businger, C. Rocken, F. Solheim, T. von Hove, R. Ware, S. McClucky, T. A. Herring, and R. W. King, 1996: GPS meteorology: Direct estimation of the absolute value of precipitable water. *J. Appl. Meteor.*, **35**, 830–838.

- Durre, I., R. S. Vose, and D. B. Wuertz, 2006: Overview of the integrated global radiosonde archive. *J. Climate*, **19**, 53–68.
- ESRL, cited 2011: NOAA/FSL Ground-Based Meteorology Site Information. [Available online at http://gpsmet.noaa.gov/test/cgi-bin/get_site_info.cgi.]
- Ferraro, R. R., F. Weng, N. Grody, and A. Basist, 1996: An eight-year (1987–1994) time series of rainfall, clouds, water vapor, snow cover, and sea ice derived from SSM/I measurements. *Bull. Amer. Meteor. Soc.*, **77**, 891–905.
- Ferraro, R. R., F. Weng, N. C. Grody, L. Zhao, H. Meng, C. Kongoli, P. Pellegrino, S. Qiu, and C. Dean, 2005: NOAA operational hydrological products derived from the Advanced Microwave Sounding Unit. *IEEE Trans. Geosci. Remote Sens.*, **43**, 1036–1049.
- Forsythe, J. M., J. B. Dodson, P. T. Partain, S. Q. Kidder, and T. H. Vonder Haar, 2012: How total precipitable water vapor anomalies relate to cloud vertical structure. *J. Hydrometeor.*, **13**, 709–721.
- Fulton, R. A., J. P. Breidenbach, D. Seo, D. A. Miller, and T. O’Bannon, 1998: The WSR-88D rainfall algorithm. *Wea. Forecasting*, **13**, 377–395.
- Graham, R. A., and R. H. Grumm, 2010: Utilizing normalized anomalies to assess synoptic-scale weather events in the western United States. *Wea. Forecasting*, **25**, 428–445.
- Greenwald, T. J., G. L. Stephens, T. H. Vonder Haar, and D. L. Jackson, 1993: A physical retrieval of cloud liquid water over the global oceans using Special Sensor Microwave/Imager (SSM/I) observations. *J. Geophys. Res.*, **98**, 18471–18488.
- Grody, N. C., A. Gruber, and W. C. Shen, 1980: Atmospheric water vapor content over the tropical Pacific derived from the Nimbus-6 scanning microwave spectrometer. *J. Appl. Meteor.*, **19**, 986–996.
- Grumm, R. H., and R. E. Hart, 2001: Standardized anomalies applied to significant cold season weather events: Preliminary findings. *Wea. Forecasting*, **16**, 736–754.
- Hart, R. E., and R. H. Grumm, 2001: Using normalized climatological anomalies to rank synoptic-scale events objectively. *Mon. Wea. Rev.*, **129**, 2426–2442.
- Hershfield, D. M., 1961: Rainfall frequency atlas of the United States. U.S. Weather Bureau Technical Paper 40, 115 pp.
- Howell, K. M., 2010: Quasi-Global and regional water vapor and rainfall rate climatologies for a 35 month period. M.S. thesis, Dept. Atmospheric Science, Colorado State University, Ft. Collins, 130 pp.

- Junker, N. W., R. S. Schneider, and S. L. Fauver, 1999: A study of heavy rainfall events during the Great Midwest Flood of 1993. *Wea. Forecasting*, **14**, 701–712.
- Junker, N. W., R. H. Grumm, R. Hart, L. F. Bosart, K. M. Bell, and F. J. Pereira, 2008: Use of normalized anomaly fields to anticipate extreme rainfall in the mountains of northern California. *Wea. Forecasting*, **23**, 336–356.
- Kanamitsu, M., W. Ebisuzaki, J. Woollen, S.-K. Yang, J. J. Hnilo, M. Fiorino, and G. L. Potter, 2002: NCEP-DEO AMIP-II Reanalysis (R-2). *Bull. Amer. Meteor. Soc.*, **83**, 1631–1643.
- Kidder, S. Q., and T. H. Vonder Haar, 1995: *Satellite Meteorology: An Introduction*. Academic Press, 466 pp.
- Kidder, S. Q., and A. S. Jones, 2007: A Blended Satellite Total Precipitable Water Product for Operational Forecasting. *J. Atmos. Oceanic Technol.*, **24**, 74–81.
- Koch, S. E., M. Desjardins, and P. J. Kocin, 1983: An interactive Barnes objective map analysis scheme for use with satellite and conventional data. *J. Climate and Appl. Meteor.*, **22**, 1487–1503.
- Lin, Y., and K. E. Mitchell, 2005: The NCEP Stage II/IV hourly precipitation analyses: development and applications. Preprints, *19th Conf. on Hydrology*, San Diego, CA, Amer. Meteor. Soc., Paper 1.2.
- Maddox, R. A., C. F. Chappell, and L. R. Hoxit, 1979: Synoptic and meso- α scale aspects of flash flood events. *Bull. Amer. Meteor. Soc.*, **60**, 115–123.
- Marshall, J., and R. A. Plumb, 2008: *Atmosphere, Ocean, and Climate Dynamics: An Introductory Text*. Elsevier Academic Press, 319 pp.
- Martin, J. E., 2006: *Mid-Latitude Atmospheric Dynamics: A First Course*. John Wiley & Sons, 324 pp.
- Meyer, C. L., 2004: Forecasting rain events in the southern Great Plains using GPS total precipitable water amounts. M.S. thesis, Dept. Atmospheric Science, Colorado State University, Ft. Collins, 114 pp.
- Moore, B. J., P. J. Neiman, F. M. Ralph, and F. Barthold, 2012: Physical processes associated with heavy flooding rainfall in Nashville, Tennessee, and vicinity during 1–2 May 2010: The role of an atmospheric river and mesoscale convective systems. *Mon. Wea. Rev.*, **140**, 358–378.
- Moore, J. T., F. H. Glass, C. E. Graves, S. M. Rochette, and M. J. Singer, 2003: The environment of warm-season elevated thunderstorms associated with heavy rainfall over the central United States. *Wea. Forecasting*, **18**, 861–878.

- Newell, R. E., N. E. Newell, Y. Zhu, and C. Scott, 1992: Tropospheric rivers? – A pilot study. *Geophys. Res. Lett.*, **19**, 2401–2404.
- Newell, R. E., and Y. Zhu, 1994: Tropospheric rivers: A one-year record and a possible application to ice core data. *Geophys. Res. Lett.*, **21**, 113–116.
- NWS, cited 2012: Hydrologic Information Center: United States Flood Loss Report – Water Year 2011. [Available online at <http://www.nws.noaa.gov/hic/summaries/WY2011.pdf>.]
- Oort, A. H., 1983: Global atmospheric circulation statistics, 1958–1973. NOAA Professional Paper No. 14, 180 pp.
- Orville, H. D., 2003: Weather Modification. *Handbook of Weather, Climate, and Water: Dynamics, Climate, Physical Meteorology, weather Systems and Measurements*, T. D. Potter and B. R. Colman, Ed., John Wiley & Sons, 433–452.
- Petty, G. W., 2008: *A First Course in Atmospheric Thermodynamics*. Sundog Publishing, 336 pp.
- Rama Varma Raja, M. K., S. I. Gutman, J. G. Yoe, L. M. McMillin, and J. Zhao, 2008: The validation of AIRS retrievals of integrated precipitable water vapor using measurements from a network of ground-based GPS receivers over the contiguous United States. *J. Atmos. Oceanic Technol.*, **25**, 416–428.
- Randel, D. L., T. H. Vonder Haar, M. A. Ringerud, G. L. Stephens, T. J. Greenwald, and C. L. Combs, 1996: A new global water vapor dataset. *Bull. Amer. Meteor. Soc.*, **77**, 1233–1246.
- Reynolds, R. W., 1988: A real-time global sea surface temperature analysis. *J. Climate*, **1**, 75–87.
- Rienecker, M. M., and Coauthors, 2011: MERRA: NASA’s Modern-Era Retrospective Analysis for Research and Applications. *J. Climate*, **24**, 3624–3648.
- Ross, R. J., and W. P. Elliot, 1996: Tropospheric water vapor climatology and trends over North America: 1973-93. *J. Climate*, **9**, 3561–3574.
- Schumacher, R. S., and R. H. Johnson, 2005: Organization and environmental properties of extreme-rain-producing mesoscale convective systems. *Mon. Wea. Rev.*, **133**, 961–976.
- Schumacher, R. S., and R. H. Johnson, 2006: Characteristics of U.S. extreme rain events during 1999–2003. *Wea. Forecasting*, **21**, 69–85.
- Shirkey, R., 2010: Army research lab tactical decision aides and related work. *Proc. 7th Conf. on Battlespace Atmospheric and Cloud Impacts on Military Operations*, Omaha, NE, U.S. Army Research Lab, P6.1.

- Simmons, K. M., and D. Sutter, 2008: Tornado warnings, lead times, and tornado casualties: An empirical investigation. *Wea. Forecasting*, **23**, 246–258.
- Smith, W. L., H. M. Woolf, C. M. Hayden, D. Q. Wark, and L. M. McMillin, 1979: The TIROS-N operational vertical sounder. *Bull. Amer. Meteor. Soc.*, **60**, 1177–1187.
- Stephens, G. L., D. L. Jackson, and J. J. Bates, 1994: A comparison of SSM/I and TOVS column water vapor data over the global oceans. *Meteor. Atmos. Phys.*, **54**, 183–201.
- Stevenson, S. N. and R. S. Schumacher, cited 2012: An analysis of 50-year and 100-year recurrence interval extreme rainfall events in the central and eastern United States. [Available online at http://schumacher.atmos.colostate.edu/research/stevenson_ams_poster_FINAL.pdf.]
- Tuller, S. E., 1968: World distribution of mean monthly and annual precipitable water. *Mon. Wea. Rev.*, **96**, 785–797.
- USACE, cited 2011: USACE, Army divers team up for solutions at Kajaki, Dahla dams in Afghanistan. [Available online at http://www.army.mil/article/64402/USACE__Army_divers_team_up_for_solutions_at_Kajaki__Dahla_dams_in_Afghanistan.]
- Vonder Haar, T. H., J. M. Forsythe, D. McKague, D. L. Randel, B. C. Ruston, and S. Woo, 2003: Continuation of the NVAP global water vapor data sets for Pathfinder science analysis. STC Tech. Rep. 3333, 43 pp.
- Waldstreicher, J. S., 2005: Assessing the impact of collaborative research projects on NWS warning performance. *Bull. Amer. Meteor. Soc.*, **86**, 193–203.
- Weng, F., L. Zhao, R. R. Ferraro, G. Poe, X. Li, and N. C. Grody, 2003: Advanced microwave sounding unit cloud and precipitation algorithms. *Radio Sci.*, **38**, 8068–8080.
- White, A. B., P. J. Neiman, F. M. Ralph, D. E. Kingsmill, and P. O. G. Persson, 2003: Coastal orographic rainfall processes observed by radar during the California Land-Falling Jets Experiment. *J. Hydrometeor.*, **4**, 264–282.
- Wilks, D. S., 2011: *Statistical Methods in the Atmospheric Sciences*. Academic Press, 704 pp.
- Wu, X., J. J. Bates, and S. J. S. Khalsa, 1993: A climatology of the water vapor band brightness temperatures from NOAA operational satellites. *J. Climate*, **6**, 1282–1300.
- Zhu, Y., and R. E. Newell, 1994: Atmospheric rivers and bombs. *Geophys. Res. Lett.*, **21**, 1999–2002.

APPENDIX I

TPWA distributions vary based on location, even within the central to eastern United States. This appendix includes the distributions of TPWA for each of the twelve forecasting locations for April through September of 2011. Distributions similar to these could be used in future work to potentially improve the performance of the forecast tool by quantifying the variance of TPWA at individual locations.

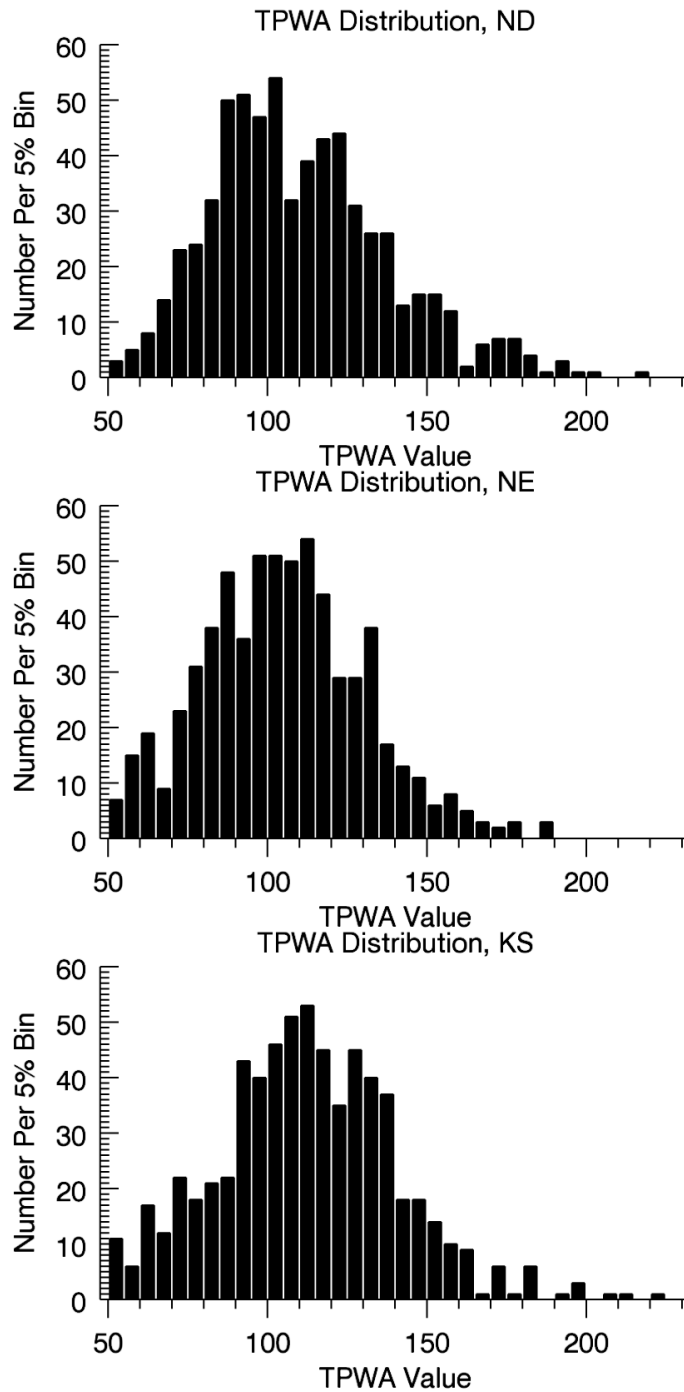


Figure A.1: TPWA distribution using 5%-width bins for the months of April through September 2011 for the North Dakota, Nebraska, and Kansas forecasting locations.

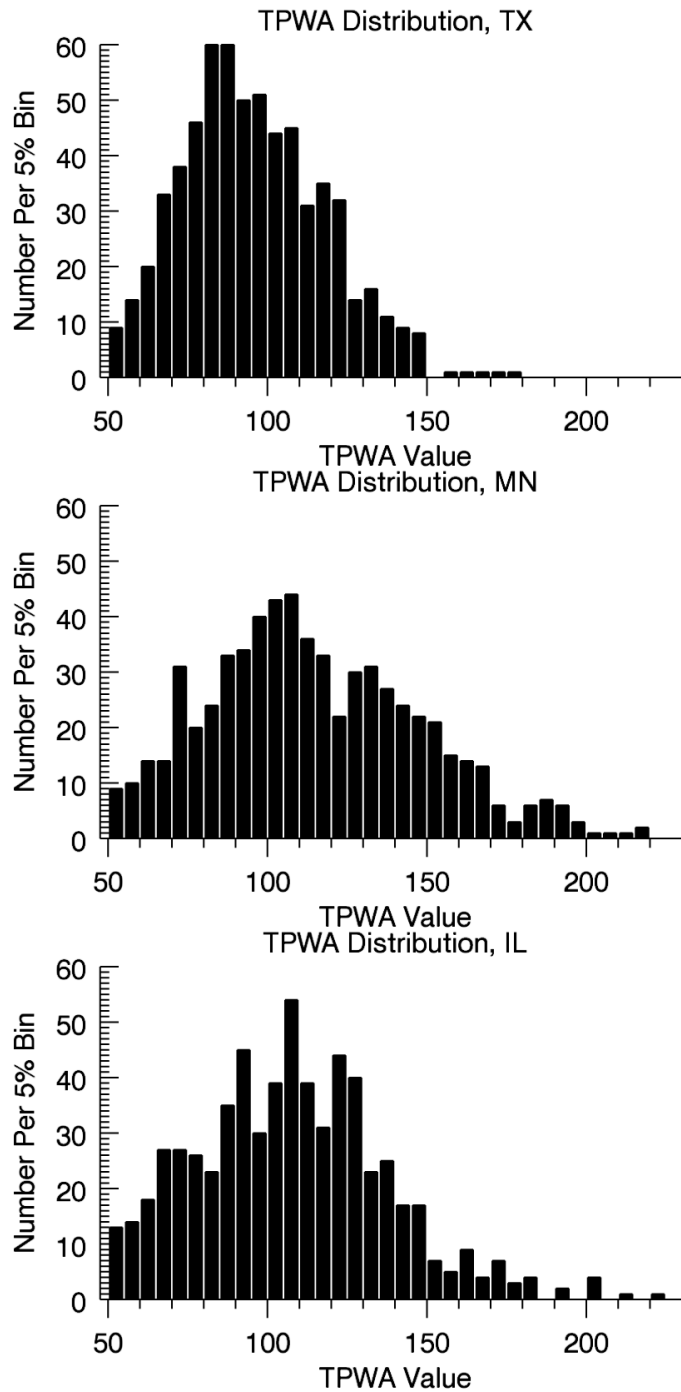


Figure A.2: TPWA distribution using 5%-width bins for the months of April through September 2011 for the Texas, Minnesota, and Illinois forecasting locations.

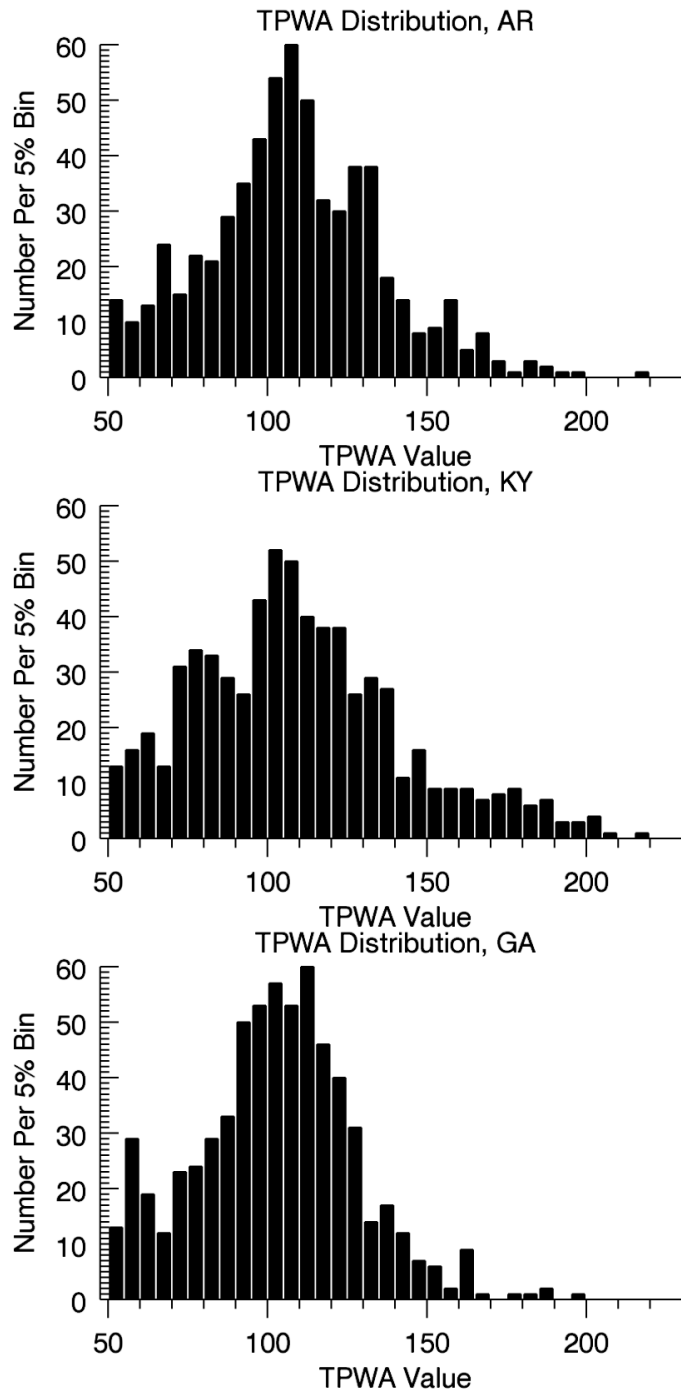


Figure A.3: TPWA distribution using 5%-width bins for the months of April through September 2011 for the Arkansas, Kentucky, and Georgia forecasting locations.

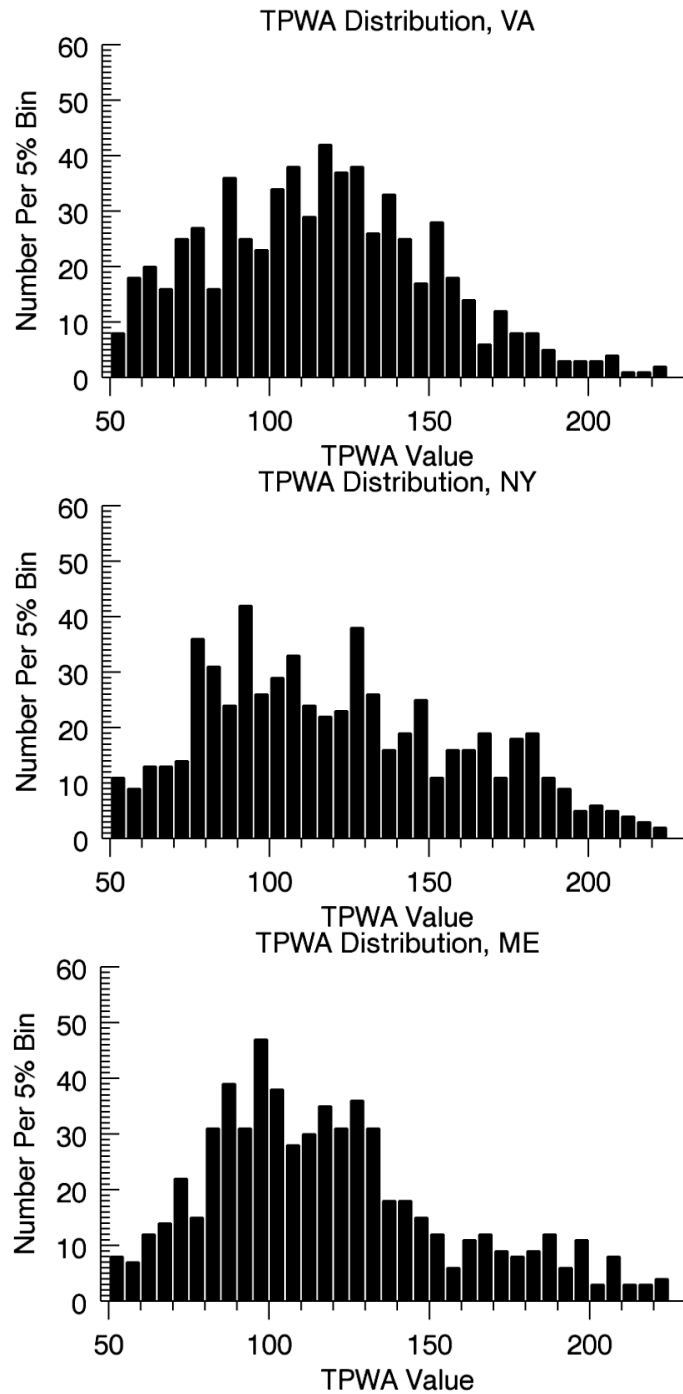


Figure A.4: TPWA distribution using 5%-width bins for the months of April through September 2011 for the Virginia, New York, and Maine forecasting locations.

LIST OF ABBREVIATIONS

AMS: American Meteorological Society

ASOS: Automated Surface Observing System

AWIPS: Advanced Weather Interactive Processing System

CIRA: Cooperative Institute for Research in the Atmosphere

CONUS: Contiguous United States of America

FAR: False Alarm Ratio

GFS: Global Forecast System

ITCZ: Intertropical Convergence Zone

LLJ: Low-Level Jet

MCS: Mesoscale Convective System. Types include:

 TL/AS: Training Line/Adjoining Stratiform

 BB: Backbuilding/Quasi-stationary

MERRA: Modern-Era Retrospective Analysis for Research and Applications

METAR: Meteorological Aerodrome Report

MIRS: Microwave Integrated Retrieval System

NASA: National Aeronautics and Space Administration

NCAR: National Center for Atmospheric Research

NCDC: National Climatic Data Center

NCEP: National Centers for Environmental Prediction

NESDIS: National Environmental Satellite, Data, and Information Service

NOAA: National Oceanic and Atmospheric Association

NVAP: NASA Water Vapor Product

NWS: National Weather Service

POD: Probability of Detection

PW: Precipitable Water. Also known as:

PRW: Precipitable Rain Water

PWAT: Precipitable Water

PWC: Precipitable Water Content

PWV: Precipitable Water Vapor

RFC: River Forecast Center

RMSE: Root-Mean-Squared Error

SSM/I: Special Sensor Microwave/Imager

SST: Sea Surface Temperature

TIROS: Television Infrared Observation Satellite

T-IWEDA: Tri-Service Integrated Weather Effects Decision Aid

TOVS: TIROS Operational Vertical Sounder

TPW: Total Precipitable Water. Also known as:

IPW: Integrated Precipitable Water

IPWV: Integrated Precipitable Water Vapor

IWV: Integrated Water Vapor

TCWV: Total Column Water Vapor

TWV: Total Water Vapor

VIM : Vertically Integrated Moisture

U.S.: United States of America / United States

UTC: Coordinated Universal Time